

# Improved $(g - 2)_\mu$ measurement and singlino dark matter in $\mu$ -term extended $\mathbb{Z}_3$ -NMSSM

---

Junjie Cao, Jingwei Lian, Yusi Pan, Di Zhang and Pengxuan Zhu

*Department of Physics, Henan Normal University, 453007, China*

*E-mail:* [junjiecao@alumni.itp.ac.cn](mailto:junjiecao@alumni.itp.ac.cn), [ljwfly@hotmail.com](mailto:ljwfly@hotmail.com),  
[panyusi0406@foxmail.com](mailto:panyusi0406@foxmail.com), [dz481655@gmail.com](mailto:dz481655@gmail.com), [zhupx99@icloud.com](mailto:zhupx99@icloud.com)

**ABSTRACT:** Very recently, a Fermilab report of muon  $g - 2$  showed a  $4.2\sigma$  discrepancy between it and the standard model (SM) prediction. Motivated by this inspiring result and the increasing tension in supersymmetric interpretation of the anomalous magnetic moment, it is argued that in the general next-to-minimal supersymmetric standard model (GSMSSM), a singlino-dominated neutralino can act as a feasible dark matter (DM) candidate in explaining the discrepancy naturally. In this case, the singlino-dominated DM and singlet-dominated Higgs bosons can form a secluded DM sector with  $\tilde{\chi}_1^0 \tilde{\chi}_1^0 \rightarrow h_s A_s$  responsible for the measured DM relic abundance when  $m_{\tilde{\chi}_1^0} \gtrsim 150$  GeV and the Yukawa coupling  $\kappa$  is around 0.2. This sector communicates with the SM sector by weak singlet-doublet Higgs mixing, so the scatterings of the singlino-dominated DM with nucleons are suppressed. Furthermore, due to the singlet nature of the DM and the complex mass hierarchy, sparticle decay chains in the GSMSSM are lengthened in comparison with the prediction of the minimal supersymmetric standard model. These characteristics lead to sparticle detection at the Large Hadron Collider (LHC) being rather tricky. This study surveys a specific scenario of the GSMSSM, which extends the  $\mathbb{Z}_3$ -NMSSM by adding an explicit  $\mu$ -term, to reveal the features. It indicates that the theory can readily explain the discrepancy of the muon anomalous magnetic moment without conflicting with the experimental results in DM and Higgs physics, and the LHC searches for sparticles.

---

## Contents

<b>1</b>	<b>Introduction</b>	<b>1</b>
<b>2</b>	<b>Theoretical preliminaries</b>	<b>3</b>
2.1	The basics of GNMSSM	3
2.2	Muon $g - 2$ in $\mu$ NMSSM	5
2.3	Singlino-dominated DM	7
<b>3</b>	<b>Explaining <math>\Delta a_\mu</math> in <math>\mu</math>NMSSM</b>	<b>10</b>
3.1	Research strategy	10
3.2	Numerical results	12
<b>4</b>	<b>LHC constraints</b>	<b>16</b>
<b>5</b>	<b>Summary</b>	<b>23</b>
<b>A</b>	<b>Fast simulation via SModelS</b>	<b>24</b>

---

## 1 Introduction

Recently, experimentalists at Fermilab National Accelerator Laboratory (FNAL) reported the most accurate measurement of the muon anomalous magnetic moment  $a_\mu^{\text{exp}}(\text{FNAL})$  [1]. Combined with the previous Brookhaven National Laboratory E821 result  $a_\mu^{\text{exp}}(\text{BNL})$  [2], the statistical average  $a_\mu^{\text{exp}}$  reads

$$\begin{aligned}a_\mu^{\text{exp}}(\text{FNAL}) &= 116592040(54) \times 10^{-11}, \\a_\mu^{\text{exp}}(\text{BNL}) &= 116592080(63) \times 10^{-11}, \\a_\mu^{\text{exp}} &= 116592061(41) \times 10^{-11},\end{aligned}\tag{1.1}$$

which reveals a  $4.2\sigma$  discrepancy with the SM prediction  $a_\mu^{\text{SM}} = 116591810(43) \times 10^{-11}$  [3–23]:

$$\Delta a_\mu = a_\mu^{\text{exp}} - a_\mu^{\text{SM}} = (251 \pm 59) \times 10^{-11}.\tag{1.2}$$

Besides, the Run-I result indicates that the future complete results of Fermilab and/or Japan Proton Accelerator Research Complex (J-PARC) experiments are very likely to confirm the excess of  $a_\mu$  at  $5\sigma$  discovery level. This expectation implies that the long-standing discrepancy of the muon anomalous magnetic moment between the SM prediction and experimental measurements,  $\Delta a_\mu$ , may be the most promising hint

of the new physics beyond the SM. As the best candidate theory for new physics, supersymmetric models predict the scalar partners of muon and  $\mu$ -type neutrino. It was speculated about twenty years ago that the source of the observed  $\Delta a_\mu$  might be the quantum effect contributed by these supersymmetric particles (sparticles) [24–26]. Along this direction, numerous studies have been carried out in the minimal supersymmetric standard model (MSSM) and its extensions (see, e.g., [27–43]).

At present, low-energy supersymmetric theories are subjected to the increasingly tight constraints from LHC experiments and DM search experiments. In the MSSM, the lightest neutralino  $\tilde{\chi}_1^0$ , if it is the lightest supersymmetric particle (LSP), can act as a DM candidate accounting for the Planck measured relic density [44]. The likelihood analysis of the phenomenological MSSM in 11 free-parameter space showed that the DM  $\tilde{\chi}_1^0$  must be bino-dominated within the  $1\sigma$  confidence level (see Figure 12 and Table 6 of Ref. [45]). Aiming at the proper recasting of the LHC Run-II data for sparticle search and assuming that  $\tilde{\chi}_1^0$  provides the full DM relic density, recent studies investigated the phenomenology of the bino DM co-annihilating with wino-dominated  $\tilde{\chi}_1^\pm$  or with sleptons  $\tilde{\ell}_{L/R}$  [46, 47]. The result revealed that it is difficult to obtain the correct DM relic density and experimentally compatible DM-nucleon scatterings in the natural parameter space to explain  $\Delta a_\mu$ <sup>1</sup>. The more recent research opened up the possibility of wino and higgsino DM by giving up  $\tilde{\chi}_1^0$  to provide the full DM relic density [48]. In the next-to minimal supersymmetric standard model with a  $\mathbb{Z}_3$  symmetry ( $\mathbb{Z}_3$ -NMSSM), which is another economic realization of supersymmetry, the DM  $\tilde{\chi}_1^0$  may be either bino-dominated or singlino-dominated [49–59]. The situation of the theory is similar to that of the MSSM, i.e., the parameter space to explain  $\Delta a_\mu$  naturally have been constrained tightly by the LHC and DM experiments [60–62].

Considering the increasing tension between natural interpretations of  $a_\mu$  and the experimental constraints, the present paper aims to study the combined constraints on the singlino-dominated DM scenario in the GNMSSM from the DM relic density, spin-dependent (SD) and spin-independent (SI) direct detection experiments, sparticle direct searches at the LHC, and the existing muon  $(g-2)$  measurement in Eq. (1.2). The rest of this paper is organized as follows. In the next section, the basics of the GNMSSM and the annihilation mechanism of singlino-dominated DM is reviewed. In Section 3, the relevant parameter space is scanned in a specific scenario of the GNMSSM, which extends the  $\mathbb{Z}_3$ -NMSSM by adding an explicit  $\mu$ -term and is called  $\mu$ NMSSM hereafter. It is found that  $(g-2)_\mu$  can be properly interpreted without conflicting with any experimental observations. In Section 4, the constraints from the LHC searches for supersymmetry on the interpretation are studied comprehensively by specific Monte Carlo simulations to reveal their features. The theory’s

---

<sup>1</sup>When we mention the term “natural” in this work, it means that higgsinos lighter than about 500 GeV are preferred to predict  $Z$  boson mass without causing serious offsets between the different contributions of  $m_Z$ .

capabilities to relax the experimental constraints are emphasized. Conclusions about the  $\mu$ NMSSM interpretation of  $\Delta a_\mu$  are drawn in Section 5.

## 2 Theoretical preliminaries

### 2.1 The basics of GNMSSM

Compared with the MSSM, the NMSSM introduces a singlet Higgs superfield  $\hat{S}$ . Given the superfield composition, the general form of the NMSSM superpotential is [63, 64]

$$W_{\text{GNMSSM}} = W_{\text{Yukawa}} + \left( \mu + \lambda \hat{S} \right) \hat{H}_u \cdot \hat{H}_d + \frac{1}{3} \kappa \hat{S}^3 + \frac{1}{2} \nu \hat{S}^2, \quad (2.1)$$

where the Yukawa terms  $W_{\text{Yukawa}}$  are the same as those in MSSM. The scenario of  $\mu = \nu = 0$  possess an accidental  $\mathbb{Z}_3$ -symmetry, and the theory is defined in a scale-invariant form. Clearly, if the dimensional parameters  $\mu$  and  $\nu$  are non-vanishing, they should be at the weak or supersymmetry-breaking scale to break the electroweak symmetry without fine-tuning. These  $\mathbb{Z}_3$  broken terms  $\mu$  and  $\nu$  are introduced in some works to solve the tadpole problem [64, 65] and the cosmological domain-wall problem [66–68]. Past studies [66, 69–72] demonstrated that the electroweak scale  $\mu$  and  $\nu$  may come from the discrete  $\mathbb{Z}_4^R$  or  $\mathbb{Z}_8^R$  symmetry breaking at high-energy scale. Furthermore, the scale-invariant  $\mathbb{Z}_3$ -NMSSM allows it to be embedded into canonical superconformal supergravity in the Jordan frame. The superconformal symmetry of matter multiplets can be broken via a non-minimal interaction  $\chi \hat{H}_u \cdot \hat{H}_d R$ , where  $R$  is the supersymmetric version of the Ricci scalar. As shown in Ref. [73], the dimensionless coupling  $\chi$  can drive inflation in the early Universe, and can also provide a  $\mu$  term correction to the  $\mathbb{Z}_3$ -NMSSM superpotential, where  $\mu = \frac{3}{2} m_{3/2} \chi$ , with  $m_{3/2}$  denoting the gravitino mass.

This work treats  $\mu$  and  $\nu$  as free theoretical input parameters, irrespective of their physical origin. Particularly for the sake of brevity without loss of generality, a specific scenario of the GNMSSM characterized by  $\nu \equiv 0$  is investigated [74]. This so-called  $\mu$ -term extended  $\mathbb{Z}_3$ -NMSSM, i.e.,  $\mu$ NMSSM, is defined by its superpotential and the soft breaking Lagrangian as follows [75, 76]

$$\begin{aligned} W_{\mu\text{NMSSM}} &= W_{\text{Yukawa}} + (\lambda \hat{S} + \mu) \hat{H}_u \cdot \hat{H}_d + \frac{1}{3} \kappa \hat{S}^3, \\ -\mathcal{L}_{\text{soft}} &= \left[ A_\lambda \lambda S H_u \cdot H_d + \frac{1}{3} A_\kappa \kappa S^3 + B_\mu \mu H_u \cdot H_d + h.c. \right] \\ &\quad + m_{H_u}^2 |H_u|^2 + m_{H_d}^2 |H_d|^2 + m_s^2 |S|^2 + \dots, \end{aligned} \quad (2.2)$$

where  $H_u$ ,  $H_d$ , and  $S$  are the scalar parts of superfields  $\hat{H}_u$ ,  $\hat{H}_d$ , and  $\hat{S}$ , respectively. After the electroweak symmetry breaking, the neutral Higgs fields acquire non-zero

vacuum expectation values (vevs),

$$\langle H_u^0 \rangle = \frac{1}{\sqrt{2}}v_u, \quad \langle H_d^0 \rangle = \frac{1}{\sqrt{2}}v_d, \quad \langle S \rangle = \frac{1}{\sqrt{2}}v_s, \quad (2.3)$$

where  $v = \sqrt{v_u^2 + v_d^2} = 246$  GeV. In practice, the free input parameters of the Higgs sector can be taken as follows<sup>2</sup>

$$\lambda, \quad \kappa, \quad A_\lambda, \quad A_\kappa, \quad \mu, \quad \mu_{\text{eff}} = \frac{1}{\sqrt{2}}\lambda v_s, \quad \tan \beta = \frac{v_u}{v_d}. \quad (2.4)$$

In the field convention that  $H_{\text{SM}} \equiv \sin \beta \text{Re}(H_u^0) + \cos \beta \text{Re}(H_d^0)$ ,  $H_{\text{NSM}} \equiv \cos \beta \text{Re}(H_u^0) - \sin \beta \text{Re}(H_d^0)$ , and  $A_{\text{NSM}} \equiv \cos \beta \text{Im}(H_u^0) - \sin \beta \text{Im}(H_d^0)$  [77, 78], the elements of the  $CP$ -even Higgs boson mass matrix  $\mathcal{M}_S^2$  in the bases  $(H_{\text{NSM}}, H_{\text{SM}}, \text{Re}(S))$  are read as

$$\begin{aligned} \mathcal{M}_{S,11}^2 &= \frac{2\mu_{\text{eff}}(\lambda A_\lambda + \kappa \mu_{\text{eff}})}{\lambda \sin 2\beta} + \frac{1}{2}(2m_Z^2 - \lambda^2 v^2) \sin^2 2\beta, \\ \mathcal{M}_{S,12}^2 &= -\frac{1}{4}(2m_Z^2 - \lambda^2 v^2) \sin 4\beta, \\ \mathcal{M}_{S,13}^2 &= -\frac{1}{\sqrt{2}}(\lambda A_\lambda + 2\kappa \mu_{\text{eff}})v \cos 2\beta, \\ \mathcal{M}_{S,22}^2 &= m_Z^2 \cos^2 2\beta + \frac{1}{2}\lambda^2 v^2 \sin^2 2\beta, \\ \mathcal{M}_{S,23}^2 &= \frac{v}{\sqrt{2}}(2\lambda \mu_{\text{eff}} + 2\lambda \mu - (\lambda A_\lambda + 2\kappa \mu_{\text{eff}}) \sin 2\beta), \\ \mathcal{M}_{S,33}^2 &= \frac{\lambda A_\lambda \sin 2\beta}{4\mu_{\text{eff}}}\lambda v^2 + \frac{\mu_{\text{eff}}}{\lambda} \left( \kappa A_\kappa + \frac{4\kappa^2 \mu_{\text{eff}}}{\lambda} \right) - \frac{\lambda \mu}{2\mu_{\text{eff}}}\lambda v^2. \end{aligned} \quad (2.5)$$

Dropping the Goldstone mode, those elements for  $CP$ -odd Higgs fields in the bases  $(A_{\text{NSM}}, \text{Im}(S))$  are given by

$$\begin{aligned} \mathcal{M}_{P,11}^2 &= \frac{2\mu_{\text{eff}}(\lambda A_\lambda + \kappa \mu_{\text{eff}})}{\lambda \sin 2\beta}, \quad \mathcal{M}_{P,12}^2 = \frac{v}{\sqrt{2}}(\lambda A_\lambda - 2\kappa \mu_{\text{eff}}), \\ \mathcal{M}_{P,22}^2 &= \frac{(\lambda A_\lambda + 4\kappa \mu_{\text{eff}}) \sin 2\beta}{4\mu_{\text{eff}}}\lambda v^2 - \frac{3\mu_{\text{eff}}}{\lambda} \kappa A_\kappa - \frac{\lambda \mu}{2\mu_{\text{eff}}}\lambda v^2. \end{aligned} \quad (2.6)$$

Three  $CP$ -even mass eigenstates  $h$ ,  $H$ , and  $h_s$  are achieved by a unitary matrix  $V$  to diagonalize  $\mathcal{M}_S^2$ . Similarly, two  $CP$ -odd mass eigenstates  $A_H$  and  $A_s$  are defined via rotation matrix  $U$ . Among them,  $h$  corresponds to the scalar state discovered at the LHC,  $H$  and  $A_H$  represent the doublet dominated states which are preferred to be heavy by the LHC search for extra Higgs bosons, and  $h_s$  and  $A_s$  represent the singlet-dominated states. The mass of the charged Higgs state  $H^\pm$  is expressed as

$$m_{H^\pm}^2 = \frac{2\mu_{\text{eff}}}{\sin 2\beta} \left( \frac{\kappa}{\lambda} \mu_{\text{eff}} + A_\lambda \right) + m_W^2 - \lambda^2 v^2. \quad (2.7)$$

---

<sup>2</sup>Since  $B_\mu$  plays a minor role in the DM phenomenology [74, 75] and muon  $g-2$ ,  $B_\mu$  is fixed as zero in this work.

The fermion parts of Higgs superfields  $(\tilde{H}_u, \tilde{H}_d, \tilde{S})$  and gauginos  $(\tilde{B}, \tilde{W})$  form five neutralino states and two chargino states, and they are referred as electroweakinos (EWinos) in general. The symmetric neutralino mass matrix in the gauge eigenstate bases of  $\psi^0 = (-i\tilde{B}, -i\tilde{W}^0, \tilde{H}_d^0, \tilde{H}_u^0, \tilde{S})$  is

$$\mathcal{M}_{\tilde{N}} = \begin{pmatrix} M_1 & 0 & -c_\beta s_W m_Z & s_\beta s_W m_Z & 0 \\ 0 & M_2 & c_\beta c_W m_Z & -s_\beta c_W m_Z & 0 \\ -c_\beta s_W m_Z & c_\beta c_W m_Z & 0 & -\mu - \mu_{\text{eff}} & -\frac{1}{\sqrt{2}} s_\beta \lambda v \\ s_\beta s_W m_Z & -s_\beta c_W m_Z & -\mu - \mu_{\text{eff}} & 0 & -\frac{1}{\sqrt{2}} c_\beta \lambda v \\ 0 & 0 & -\frac{1}{\sqrt{2}} s_\beta \lambda v & -\frac{1}{\sqrt{2}} c_\beta \lambda v & \frac{2\kappa}{\lambda} \mu_{\text{eff}} \end{pmatrix}, \quad (2.8)$$

where the abbreviations  $s_W = \sin \theta_W$  and  $c_W = \cos \theta_W$  are used, with  $\theta_W$  being the weak mixing angle, and  $s_\beta = \sin \beta$  and  $c_\beta = \cos \beta$ . Similarly, the chargino mass matrix in the bases  $\psi^\pm = (\tilde{W}^+, \tilde{H}_u^+, \tilde{W}^-, \tilde{H}_d^-)$  is

$$\mathcal{M}_{\tilde{C}} = \begin{pmatrix} 0_{2 \times 2} & X_{2 \times 2}^T \\ X_{2 \times 2} & 0_{2 \times 2} \end{pmatrix}, \quad \text{with} \quad X_{2 \times 2} = \begin{pmatrix} M_2 & \sqrt{2} s_\beta m_W \\ \sqrt{2} c_\beta m_W & \mu + \mu_{\text{eff}} \end{pmatrix}. \quad (2.9)$$

After diagonalization, one arrives at the neutralino  $\tilde{\chi}_i^0$  and chargino  $\tilde{\chi}_i^\pm$  as mass eigenstates, with increasing mass for a higher label  $i$ .

The smuon mass matrix in the gauge eigenstate bases  $(\tilde{\mu}_L, \tilde{\mu}_R)$  is given as

$$\mathcal{M}_{\tilde{\mu}}^2 = \begin{pmatrix} m_\mu^2 + m_{\tilde{\mu}_L}^2 + (s_W^2 - \frac{1}{2})m_Z^2 \cos 2\beta & m_\mu [A_\mu - (\mu + \mu_{\text{eff}}) \tan \beta] \\ m_\mu [A_\mu - (\mu + \mu_{\text{eff}}) \tan \beta] & m_\mu^2 + m_{\tilde{\mu}_R}^2 - s_W^2 m_Z^2 \cos 2\beta \end{pmatrix}, \quad (2.10)$$

where  $A_\mu$ ,  $m_{\tilde{\mu}_L}$ , and  $m_{\tilde{\mu}_R}$  are muon-type soft breaking parameters. Eq. (2.10) indicates that the left-right mixing term is dominated by  $(\mu + \mu_{\text{eff}}) \tan \beta$ , so  $A_\mu$  is fixed as zero in the following. The muon-type sneutrino mass is

$$m_{\tilde{\nu}_\mu}^2 = m_{\tilde{\mu}_L}^2 + \frac{1}{2} m_Z^2 \cos 2\beta. \quad (2.11)$$

## 2.2 Muon $g - 2$ in $\mu$ NMSSM

The SUSY contribution  $a_\mu^{\text{SUSY}}$ , in which the muon lepton number is carried by  $\tilde{\mu}$  or  $\tilde{\nu}_\mu$  in the loops<sup>3</sup>, can be the source of  $\Delta a_\mu$  [24, 93, 94]. The expression of  $a_\mu^{\text{SUSY}}$  in

---

<sup>3</sup>In the NMSSM, besides the contributions from the SM particles in the loops, heavy doublet-dominated Higgs bosons can also mediate the contribution to  $a_\mu$ . However, after considering the constraints from the LHC searches for extra Higgs bosons and the measurements of the branching ratios for  $B \rightarrow X_s \gamma$  and  $B_s \rightarrow \mu^+ \mu^-$ , this contribution is negligibly small because the Higgs bosons should be very massive for a large  $\tan \beta$ . In addition, although the contribution from light singlet-dominated Higgs bosons might reach  $\mathcal{O}(10^{-10})$  as pointed out in [79], it is negligible in this study. The reason is that the constraints from the DM direct detection experiments strongly favor a small  $\lambda$  for a singlino-dominated DM, and consequently, the singlet-doublet Higgs mixings and

the  $\mu$ NMSSM is similar to that in the MSSM [79], which is given by [24]:

$$\begin{aligned}
a_\mu^{\text{SUSY}} &= a_\mu^{\tilde{\chi}^0 \tilde{\mu}} + a_\mu^{\tilde{\chi}^\pm \tilde{\nu}}, \\
a_\mu^{\tilde{\chi}^0 \tilde{\mu}} &= \frac{m_\mu}{16\pi^2} \sum_{i,l} \left\{ -\frac{m_\mu}{12m_{\tilde{\mu}l}^2} (|n_{il}^L|^2 + |n_{il}^R|^2) F_1^N(x_{il}) + \frac{m_{\tilde{\chi}_i^0}}{3m_{\tilde{\mu}l}^2} \text{Re}(n_{il}^L n_{il}^R) F_2^N(x_{il}) \right\}, \\
a_\mu^{\tilde{\chi}^\pm \tilde{\nu}} &= \frac{m_\mu}{16\pi^2} \sum_k \left\{ \frac{m_\mu}{12m_{\tilde{\nu}k}^2} (|c_k^L|^2 + |c_k^R|^2) F_1^C(x_k) + \frac{2m_{\tilde{\chi}_k^\pm}}{3m_{\tilde{\nu}k}^2} \text{Re}(c_k^L c_k^R) F_2^C(x_k) \right\},
\end{aligned} \tag{2.12}$$

where  $i = 1, \dots, 5$ ,  $k = 1, 2$ , and  $l = 1, 2$  denote the neutralino, chargino, and smuon index, respectively, and

$$\begin{aligned}
n_{il}^L &= \frac{1}{\sqrt{2}} (g_2 N_{i2} + g_1 N_{i1}) X_{l1}^* - y_\mu N_{i3} X_{l2}^*, \quad n_{il}^R = \sqrt{2} g_1 N_{i1} X_{l2} + y_\mu N_{i3} X_{l1}, \\
c_k^L &= -g_2 V_{k1}^c, \quad c_k^R = y_\mu U_{k2}^c.
\end{aligned} \tag{2.13}$$

Here,  $N$  is the neutralino mass rotation matrix,  $X$  the smuon mass rotation matrix, and  $U^c$  and  $V^c$  the chargino mass rotation matrices defined by  $U^{c*} X_{2 \times 2} V^{c\dagger} = m_{\tilde{\chi}^\pm}^{\text{diag}}$ . The kinematic loop functions  $F(x)$ s depend on the variables  $x_{il} \equiv m_{\tilde{\chi}_i^0}^2/m_{\tilde{\mu}l}^2$  and  $x_k \equiv m_{\tilde{\chi}_k^\pm}^2/m_{\tilde{\nu}k}^2$ , and are given by

$$F_1^N(x) = \frac{2}{(1-x)^4} [1 - 6x + 3x^2 + 2x^3 - 6x^2 \ln x], \tag{2.14}$$

$$F_2^N(x) = \frac{3}{(1-x)^3} [1 - x^2 + 2x \ln x], \tag{2.15}$$

$$F_1^C(x) = \frac{2}{(1-x)^4} [2 + 3x - 6x^2 + x^3 + 6x \ln x], \tag{2.16}$$

$$F_2^C(x) = -\frac{3}{2(1-x)^3} [3 - 4x + x^2 + 2 \ln x]. \tag{2.17}$$

They satisfy  $F_1^N(1) = F_2^N(1) = F_1^C(1) = F_2^C(1) = 1$  for mass-degenerate sparticle case.

It is instructive to point out that, although the  $\mu$ NMSSM predicts five neutralinos, the singlino-induced contribution never makes sense, and the  $\mu$ NMSSM prediction of  $a_\mu^{\text{SUSY}}$  is roughly the same as that of the MSSM except that the  $\mu$  parameter of the MSSM should be replaced by  $\mu + \mu_{eff}$ . This feature can be understood by noting the fact that the field operator for  $a_\mu$  involves chiral flipped Muon leptons and adopting the mass insertion approximation in the calculation of  $a_\mu$  [93]. Specifically, the contributions to  $a_\mu^{\text{SUSY}}$  in the MSSM can be classified into four types: "WHL",

---

their related  $\bar{\mu}\mu A_s$  and  $\bar{\mu}\mu h_s$  couplings are suppressed significantly. It was testified numerically that the total Higgs-mediated contributions are less than  $10^{-10}$  for the samples obtained in this study. Besides,  $a_\mu^{\text{SUSY}}$  has two-loop contribution [80–91]. A recent analysis revealed that the correction is less than  $4 \times 10^{-10}$  [92]. We anticipate that it can be further suppressed if the restrictions from the LHC search for SUSY and DM physics are considered.

"BHL", "BHR", and "BLR", where  $W$ ,  $B$ ,  $H$ ,  $L$ , and  $R$  stands for wino, bino, higgsino, left-handed and right-handed smuon field, respectively. They arise from the Feynman diagrams involving  $\tilde{W} - \tilde{H}_d$ ,  $\tilde{B} - \tilde{H}_d^0$ ,  $\tilde{B} - \tilde{H}_d^0$ , and  $\tilde{\mu}_L - \tilde{\mu}_R$  transitions, respectively. Their concrete expressions are [93, 95, 96]

$$a_{\mu, \text{WHL}}^{\text{SUSY}} = \frac{\alpha_2 m_\mu^2 M_2 \tan \beta}{8\pi m_{\tilde{\nu}_\mu}^4} \left\{ 2f_C \left( \frac{M_2^2}{m_{\tilde{\nu}_\mu}^2}, \frac{\mu^2}{m_{\tilde{\nu}_\mu}^2} \right) - \frac{m_{\tilde{\nu}_\mu}^4}{m_{\tilde{\mu}_L}^4} f_N \left( \frac{M_2^2}{m_{\tilde{\mu}_L}^2}, \frac{\mu^2}{m_{\tilde{\mu}_L}^2} \right) \right\}, \quad (2.18)$$

$$a_{\mu, \text{BHL}}^{\text{SUSY}} = \frac{\alpha_Y m_\mu^2 M_1 \tan \beta}{8\pi m_{\tilde{\mu}_L}^4} f_N \left( \frac{M_1^2}{m_{\tilde{\mu}_L}^2}, \frac{\mu^2}{m_{\tilde{\mu}_L}^2} \right), \quad (2.19)$$

$$a_{\mu, \text{BHR}}^{\text{SUSY}} = -\frac{\alpha_Y m_\mu^2 M_1 \tan \beta}{4\pi m_{\tilde{\mu}_R}^4} f_N \left( \frac{M_1^2}{m_{\tilde{\mu}_R}^2}, \frac{\mu^2}{m_{\tilde{\mu}_R}^2} \right), \quad (2.20)$$

$$a_{\mu, \text{BLR}}^{\text{SUSY}} = \frac{\alpha_Y m_\mu^2 M_1 \tan \beta}{4\pi M_1^4} f_N \left( \frac{m_{\tilde{\mu}_L}^2}{M_1^2}, \frac{m_{\tilde{\mu}_R}^2}{M_1^2} \right), \quad (2.21)$$

where the loop functions are given by

$$f_C(x, y) = \frac{5 - 3(x + y) + xy}{(x - 1)^2(y - 1)^2} - \frac{2 \ln x}{(x - y)(x - 1)^3} + \frac{2 \ln y}{(x - y)(y - 1)^3}, \quad (2.22)$$

$$f_N(x, y) = \frac{-3 + x + y + xy}{(x - 1)^2(y - 1)^2} + \frac{2x \ln x}{(x - y)(x - 1)^3} - \frac{2y \ln y}{(x - y)(y - 1)^3}, \quad (2.23)$$

and they satisfy  $f_C(1, 1) = 1/2$  and  $f_N(1, 1) = 1/6$ . In the  $\mu\text{NMSSM}$ , the singlino field  $\tilde{S}$  can also enter the insertions, but because both the  $\tilde{W} - \tilde{S}$  and  $\tilde{B}^0 - \tilde{S}$  transitions and the  $\tilde{\mu}\tilde{S}\tilde{\mu}_{L,R}$  couplings vanish, it only appears in the "WHL", "BHL" and "BHR" loops by two more insertions at the lowest order, which corresponds to the  $\tilde{H}_d^0 - \tilde{S}$  and  $\tilde{S} - \tilde{H}_d^0$  transitions in the neutralino mass matrix in Eq. (2.8), respectively. Since a massive singlino and a small  $\lambda$  are preferred by DM physics (see discussion below), the singlino-induced contribution can not be significantly large<sup>4</sup>.

It should be emphasized that, although  $a_\mu^{\text{SUSY}}$  has roughly the same properties in the  $\mu\text{NMSSM}$  and  $\text{MSSM}$ , it is subject to significantly relaxed experimental and theoretical limitations in the  $\mu\text{NMSSM}$  (see following discussions). Thus, the  $\mu\text{NMSSM}$  is more readily to explain the  $a_\mu$  discrepancy, which is the main motivation of this work. In addition, the WHL contribution is usually much larger than the other contributions if  $\tilde{\mu}_L$  is not significantly heavier than  $\tilde{\mu}_R$ .

### 2.3 Singlino-dominated DM

This work aims to reveal DM physics in the natural parameter space of interpreting  $\Delta a_\mu$ . In the  $\mathbb{Z}_3\text{-NMSSM}$ , the properties of the singlino-dominated DM are mainly

---

<sup>4</sup>In fact, we performed a comprehensive study about the characteristics of the samples that survive all the experimental constraints. We found that, for all the sample obtained in this work, resetting  $\lambda = 0.001$  (note that the finiteness of  $m_{\tilde{S}}$  requires  $\lambda \neq 0$ ) and keeping the other parameters unchanged increase  $a_\mu^{\text{SUSY}}$  by less than 10%.



determined by three parameters:  $\lambda$ ,  $\mu$ , and  $m_{\tilde{\chi}_1^0}$  [62]. The Yukawa coupling  $\kappa$  is related with  $m_{\tilde{\chi}_1^0}$  and satisfies  $2|\kappa| < \lambda$  to ensure that  $\tilde{\chi}_1^0$  is singlino-dominated. The DM obtained the correct relic abundance mainly through co-annihilation with higgsinos in the early Universe, and  $\lambda$  should be less than 0.1 to suppress the DM direct detection rate [61, 62]. As a result, the parameters in the  $\mathbb{Z}_3$ -NMSSM are highly constrained. In contrast, due to the introduction of the additional  $\mu$  term in the  $\mu$ NMSSM, the DM properties are described by four Higgs parameters:  $\lambda$ ,  $\kappa$ ,  $\mu$ , and  $m_{\tilde{\chi}_1^0} \simeq \frac{2\kappa}{\lambda}\mu_{\text{eff}}$ , and a singlino-dominated DM does not require  $2|\kappa| < \lambda$  [74]. This causes the singlino-dominated DM properties in the  $\mu$ NMSSM to be significantly different from those in the  $\mathbb{Z}_3$ -NMSSM.

Assuming a standard thermal history of the Universe with a singlino-dominated DM candidate in thermal equilibrium until it freezed out, DM annihilation rate must be sufficiently large to be consistent with the Planck observation  $\Omega_{\text{DM}}h^2 = 0.120 \pm 0.001$ . Various processes, as follows, may provide a sufficiently large annihilation cross-section [74].

- $\tilde{\chi}_1^0\tilde{\chi}_1^0 \rightarrow h_s A_s$ . This process is mainly carried out through  $s$ -channel exchange of  $Z$  and  $CP$ -odd Higgs  $A_s$  and  $t$ -channel exchange of neutralinos [52, 97]. As shown in Eq. (2.19) in [74], the  $t$ -channel annihilation cross-section is roughly proportional to  $\kappa^4$ . In the  $t$ -channel dominated case, the parameters should satisfy the relationship [52]

$$|\kappa| \sim 0.15 \times \left( \frac{m_{\tilde{\chi}_1^0}}{300 \text{ GeV}} \right)^{1/2} \quad (2.24)$$

to obtain the measured density. For the case of  $m_{A_s} \simeq 2 \times m_{\tilde{\chi}_1^0}$ , the cross-section is enhanced by the  $s$ -channel pole. However, the  $A_s$  pole enhancement may lead to a very light singlet Higgs boson  $h_s$ . This  $h_s$  must satisfy the constraints from LEP Higgs searches and predict a small  $\text{BR}(h \rightarrow h_s h_s)$  to fit SM-like Higgs data. Besides, the SI direct detection rate mediated by  $h_s$  must satisfy the current bound from Xenon-1T [98] and PandaX-II [99]. A comparative study of light  $h_s$  scenario ( $m_{h_s} < m_h$ ) and heavy  $h_s$  scenario ( $m_{h_s} > m_h$ ) indicated that the latter scenario is preferred by a Bayes factor 2.42 [74]<sup>5</sup>. For the above reasons, only the  $m_{h_s} > m_h$  scenario will be considered (i.e.,  $h_1 = h$  and  $h_2 = h_s$ ) in the following numerical study.

- $\tilde{\chi}_1^0\tilde{\chi}_1^0 \rightarrow t\bar{t}$ . This process is mediated by the  $s$ -channel exchange of  $Z$  and Higgs bosons. It is significant only when  $\lambda$  is sizable, but this usually leads to a sizable DM-nucleon scattering rate [62].

---

<sup>5</sup>A Bayes factor is the ratio of the likelihood of one particular hypothesis to the likelihood of another. It can be interpreted as a measure of the strength of evidence in favor of one theory among two competing theories [100, 101]. A factor of 2.42 is generally considered as a decisive result to indicate the preference of one theory over another.

- Co-annihilation with EWinos. In principle, this channel affects the abundance when the mass splitting between  $\tilde{\chi}_1^0$  and a co-annihilation particle is less than approximately 10% [62].
- Co-annihilation with smuons  $\tilde{\mu}_L/\tilde{\mu}_R$  or  $\mu$ -type sneutrino  $\tilde{\nu}_\mu$ . Within the interpretation of  $\Delta a_\mu$ , smuons should not be too heavy, so this co-annihilation channel can be opened when  $m_{\tilde{\mu}} \gtrsim m_{\tilde{\chi}_1^0}$ .

In the heavy squark limits, SI DM-nucleon scattering is mainly from  $t$ -channel exchange of  $CP$ -even Higgs bosons, and the cross-section is given as [102, 103]

$$\sigma_N^{\text{SI}} = \frac{4\mu_r^2}{\pi} |f^{(N)}|^2, \quad f^{(N)} = \sum_i^3 f_{h_i}^{(N)} = \sum_i^3 \frac{C_{\tilde{\chi}_1^0 \tilde{\chi}_1^0 h_i} C_{NNh_i}}{2m_{h_i}^2}, \quad (2.25)$$

where  $\mu_r = m_N m_{\tilde{\chi}_1^0} / (m_N + m_{\tilde{\chi}_1^0})$  is the reduced mass of the DM-nucleon system, and  $C_{NNh_i}$  is the coupling of a Higgs boson with a nucleon,

$$C_{NNh_i} = -\frac{m_N}{v} \left( F_d^{(N)} (V_{i2} - \tan \beta V_{i1}) + F_u^{(N)} \left( V_{i2} + \frac{1}{\tan \beta} V_{i1} \right) \right). \quad (2.26)$$

Here  $F_d^{(N)} = f_d^{(N)} + f_s^{(N)} + \frac{2}{27} f_G^{(N)}$  and  $F_u^{(N)} = f_u^{(N)} + \frac{4}{27} f_G^{(N)}$  with form factor  $f_q^{(N)} = m_N^{-1} \langle N | m_q q \bar{q} | N \rangle$  and  $f_G^{(N)} = 1 - \sum_{q=u,d,s} f_q^{(N)}$ . In the heavy  $H$  case, the SI cross-section is dominated by two light Higgs contributions, and the  $h$ -mediated contribution is usually significantly larger than the  $h_s$ -mediated contribution. The couplings  $C_{\tilde{\chi}_1^0 \tilde{\chi}_1^0 h}$  and  $C_{\tilde{\chi}_1^0 \tilde{\chi}_1^0 h_s}$  are given by [74]

$$\begin{aligned} C_{\tilde{\chi}_1^0 \tilde{\chi}_1^0 h} &\simeq \frac{\mu + \mu_{\text{eff}}}{v} \left( \frac{\lambda v}{\mu + \mu_{\text{eff}}} \right)^2 \frac{N_{15}^2 V_{12} (m_{\tilde{\chi}_1^0} / (\mu + \mu_{\text{eff}}) - \sin 2\beta)}{1 - (m_{\tilde{\chi}_1^0} / (\mu + \mu_{\text{eff}}))^2} \\ &\quad + \frac{\lambda}{2\sqrt{2}} \left( \frac{\lambda v}{\mu + \mu_{\text{eff}}} \right)^2 \frac{N_{15}^2 V_{13} \sin 2\beta}{1 - (m_{\tilde{\chi}_1^0} / (\mu + \mu_{\text{eff}}))^2} \\ &\quad - \sqrt{2} \kappa N_{15}^2 V_{13} \left[ 1 + \left( \frac{\lambda v}{\sqrt{2}(\mu + \mu_{\text{eff}})} \right)^2 \frac{1}{1 - (m_{\tilde{\chi}_1^0} / (\mu + \mu_{\text{eff}}))^2} \frac{\mu_{\text{eff}}}{\mu + \mu_{\text{eff}}} \right], \\ C_{\tilde{\chi}_1^0 \tilde{\chi}_1^0 h_s} &\simeq \frac{\mu + \mu_{\text{eff}}}{v} \left( \frac{\lambda v}{\mu + \mu_{\text{eff}}} \right)^2 \frac{N_{15}^2 V_{22} (m_{\tilde{\chi}_1^0} / (\mu + \mu_{\text{eff}}) - \sin 2\beta)}{1 - (m_{\tilde{\chi}_1^0} / (\mu + \mu_{\text{eff}}))^2} \\ &\quad + \frac{\lambda}{2\sqrt{2}} \left( \frac{\lambda v}{\mu + \mu_{\text{eff}}} \right)^2 \frac{N_{15}^2 V_{23} \sin 2\beta}{1 - (m_{\tilde{\chi}_1^0} / (\mu + \mu_{\text{eff}}))^2} \\ &\quad - \sqrt{2} \kappa N_{15}^2 V_{23} \left[ 1 + \left( \frac{\lambda v}{\sqrt{2}(\mu + \mu_{\text{eff}})} \right)^2 \frac{1}{1 - (m_{\tilde{\chi}_1^0} / (\mu + \mu_{\text{eff}}))^2} \frac{\mu_{\text{eff}}}{\mu + \mu_{\text{eff}}} \right]. \end{aligned} \quad (2.27)$$

In contrast, the SD scattering cross-section takes the following simple form from [104, 105]:

$$\begin{aligned} \sigma_N^{\text{SD}} &\simeq C_N \times 10^{-4} \text{ pb} \times \left( \frac{N_{13}^2 - N_{14}^2}{0.1} \right)^2, \\ &\simeq C_N \times 10^{-2} \text{ pb} \times \left( \frac{\lambda v}{\sqrt{2}(\mu + \mu_{\text{eff}})} \right)^4 \left( \frac{N_{15}^2 \cos 2\beta}{1 - (m_{\tilde{\chi}_1^0} / (\mu + \mu_{\text{eff}}))^2} \right)^2, \end{aligned} \quad (2.28)$$

with  $C_p \simeq 4.0$  for the proton and  $C_n \simeq 3.1$  for the neutron. The above formulae indicate that the DM direct detection rate is positively related to the Higgs coupling  $\lambda$ , roughly in terms of  $\lambda v/(\sqrt{2}(\mu + \mu_{eff}))$ .

### 3 Explaining $\Delta a_\mu$ in $\mu$ NMSSM

#### 3.1 Research strategy

The following relevant parameter space was scanned using the **MultiNest** technique with the setting  $n_{\text{live}} = 30000$  [106, 107]<sup>6</sup> to explore the features of the  $\mu$ NMSSM interpretation of  $\Delta a_\mu$ :

$$\begin{aligned} |M_1| &\leq 1.5 \text{ TeV}, \quad 100 \text{ GeV} \leq M_2 \leq 1.5 \text{ TeV}, \\ 0 &\leq \lambda \leq 0.5, \quad |\kappa| \leq 0.5, \quad 1 \leq \tan \beta \leq 60, \quad 2 \text{ TeV} \leq A_t \leq 5 \text{ TeV}, \\ 10 \text{ GeV} &\leq \mu \leq 1 \text{ TeV}, \quad 100 \text{ GeV} \leq \mu + \mu_{\text{eff}} \leq 1 \text{ TeV}, \quad |A_\kappa| \leq 700 \text{ GeV}, \\ 100 \text{ GeV} &\leq m_{\tilde{\mu}_L} \leq 1 \text{ TeV}, \quad 100 \text{ GeV} \leq m_{\tilde{\mu}_R} \leq 1 \text{ TeV}. \end{aligned} \quad (3.1)$$

All of the input parameters are flatly distributed beforehand. Other SUSY parameters, such as  $A_\lambda$ , the parameters for the first and third generation sleptons, three generation squarks, and gluino, are fixed at 2 TeV. In the numerical calculation, the model file of the  $\mu$ NMSSM is constructed through the package **SARAH-4.14.3** [108–111]. The particle mass spectra and low-energy observables, such as  $a_\mu^{\text{SUSY}}$ , are generated by the codes **SPheno-4.0.3** [112, 113] and **FlavorKit** [114]. The DM relic density and direct detection cross-sections are calculated using package **MicrOMEGAs-5.0.4** [115–120]. The following likelihood function

$$\mathcal{L} = \begin{cases} \exp \left[ -\frac{1}{2} \left( \frac{a_\mu^{\text{SUSY}} - 2.51 \times 10^{-9}}{5.9 \times 10^{-10}} \right)^2 \right], & \text{if restrictions satisfied;} \\ \exp[-100], & \text{if restrictions unsatisfied.} \end{cases} \quad (3.2)$$

was constructed to guide the scan, where the restrictions on each sample include:

- Higgs data fit. As mentioned above, the lightest  $CP$ -even Higgs boson  $h_1$  corresponds to the SM-like state, and this state must satisfy the constraints from the LHC data using the code **HiggsSignal-2.2.3** [121]. The  $p$  value in the fit is required to be larger than 0.05, which implies that the Higgs property coincides with the data at the 95% confidence level. The extra Higgs states must pass the constraints from the direct searches at the LEP, Tevatron, and LHC, which is implemented by the code **HiggsBounds-5.3.2** [122].

---

<sup>6</sup>The parameter  $n_{\text{live}}$  in the MultiNest algorithm denotes the number of active or live points used to determine the iso-likelihood contours in each iteration [106, 107]. The larger it is, the more accurate the results, and correspondingly, more samples are obtained in the scan.

- Constraints from  $B$ -physics observation  $\text{BR}(B_s \rightarrow \mu^+ \mu^-)$  and  $\text{BR}(B_s \rightarrow X_s \gamma)$  are taken into consideration [100]. These two  $B$ -physics observables must fall into the  $2\sigma$  bounds.
- DM relic density constraints. The samples are required to have a neutralino LSP, and the predicted relic density of samples must agree with the Planck measurement [44]<sup>7</sup>, i.e.,  $0.096 \leq \Omega h^2 \leq 0.144$ .
- Direct detection limits on DM. The SI DM scattering cross-section  $\sigma_p^{\text{SI}}$  is required to be below the constraint from the Xenon-1T experiment [98]. The SD cross-section  $\sigma_n^{\text{SD}}$  is needed to pass the limits of the Xenon-1T report [123].
- Constraints from LHC sparticles direct searches. In the  $\mu\text{NMSSM}$  explanation of  $\Delta a_\mu$ , the EWinos and sleptons can be produced at the LHC, and thus restricted by the searches for multi-lepton signals. The constraints implemented in this step are produced using the code `SModelS-1.2.3` [124], which contained the experimental analyses in simplified models that are summarized in Appendix A.

For each sample obtained in the scan, the stability of its vacuum for the scalar potential consisting of Higgs and the last two generation slepton fields was finally checked by the code `Vevacious` [125, 126]. Compared with the MSSM, the vacuum in the  $\mu\text{NMSSM}$  is more stable due to the addition of the singlet Higgs field as dynamical degree of freedom, especially in the case of a small  $\lambda$  and a large  $\mu_{\text{eff}}$  [75], but tremendously large soft-breaking trilinear coefficients may still cause its destabilization [127]. Generally speaking, the vacuum destabilization occurs in the following situations:

- One or more tachyonic Higgs masses are predicted. Tachyonic masses are related to the fact that the electroweak point, around which the potential is expanded, is not a local minimum in the scalar potential, but rather resembles a saddle point or even a local maximum [75]. In this case, the true vacuum lies at a deeper point along this tachyonic direction. Consequently, the true vacuum has vevs different from the input values, and the electroweak breaking condition does not select a minimum.

In this study, it was found that more than half of the samples encountered in the scan correspond to the tachyonic mass case. They are abandoned directly in the calculation since they can not predict physical mass spectra.

- The formation of non-standard minima which break the electric and/or color charges, known as charge- and color-breaking (CCB) minima. In the MSSM,

---

<sup>7</sup>Note that the uncertainty of  $\Omega h^2$  is dominated by the 10% theoretical uncertainties in calculating the density, which are much larger than the uncertainty of the Planck measurement.

the following condition should be satisfied to avoid the CCB vacuum [128, 129]:

$$|y_{\ell,\text{eff}}\mu v \tan \beta| \leq \eta_\ell \left[ 1.01 \times 10^2 \text{GeV} \sqrt{m_{\tilde{\ell}_L} m_{\tilde{\ell}_R}} + 1.01 \times 10^2 \text{GeV} (m_{\tilde{\ell}_L} + 1.03 m_{\tilde{\ell}_R}) - 2.27 \times 10^4 \text{GeV}^2 + \frac{2.97 \times 10^6 \text{GeV}^3}{m_{\tilde{\ell}_L} + m_{\tilde{\ell}_R}} - 1.14 \times 10^8 \text{GeV}^4 \left( \frac{1}{m_{\tilde{\ell}_L}^2} + \frac{0.983}{m_{\tilde{\ell}_R}^2} \right) \right], \quad (3.3)$$

where  $y_{\ell,\text{eff}}$  with  $\ell = \tau, \mu$  are the lepton Yukawa couplings including radiative corrections [130],  $\eta_\tau \simeq 1$  and  $\eta_\mu \simeq 0.88$ . If the singlet-field direction were neglected, the formula could be directly applied to the  $\mu\text{NMSSM}$ , keeping  $v_s \neq 0$  GeV and replacing  $\mu \rightarrow \mu + \mu_{eff}$ . However, with the singlet as dynamical degree of freedom, the stability of the electroweak vacuum is improved as the only singlet–slepton contribution is actually a quadrilinear term  $\lambda Y_\ell S H_u^0 \tilde{\ell}_L^* \tilde{\ell}_R$ , and the occurrence of a vacuum with  $\langle \tilde{\ell}_L \rangle \neq 0$  and  $\langle \tilde{\ell}_R \rangle \neq 0$  can enhance the scalar potential [75].

It should be pointed out that, for the parameter space in Eq. (3.1), samples obtained in the scan satisfy the inequality automatically. The reason is the ATLAS measurement of the properties of the discovered Higgs particle has required  $0.77 \leq Y_{\tau,\text{eff}}/Y_{\tau,\text{SM}} \leq 1.37$  [131] and  $Y_{\mu,\text{eff}}/Y_{\mu,\text{SM}} \leq 2.4$  [132] at  $2\sigma$  confidence level. This conclusion translates the inequality into simple forms:  $(\mu + \mu_{eff}) \tan \beta \lesssim 2.5 \times 10^5$  GeV for  $\tilde{\tau}$ -Higgs potential, and  $(\mu + \mu_{eff}) \tan \beta \lesssim 1.9 \times 10^5$  GeV for  $\tilde{\mu}$ -Higgs potential with  $m_{\tilde{\mu}_L} = m_{\tilde{\mu}_R} = 200$  GeV. For  $\tan \beta = 60$ , they read  $(\mu + \mu_{eff}) \lesssim 4.2 \times 10^3$  GeV and  $(\mu + \mu_{eff}) \lesssim 3.1 \times 10^3$  GeV, respectively. In fact, our calculation with the code Vevacious found no CCB global minima in the scan.

- The electroweak vacuum of the sample, which was called the desired symmetry breaking (DSB) vacuum in literature [75, 127], corresponds to a local minimum of the scalar potential instead of a global minimum. In this case, the DSB vacuum could undergo quantum tunneling to the true vacuum. If the tunneling time is short enough in reference to the age of Universe, the DSB vacuum would decay completely [125, 126]. Such vacuum was called metastable but short-lived. Evidently, the occurrence of the metastable vacuum depends on the contour of the scalar potential, which is mainly decided by the parameters  $\lambda$ ,  $\kappa$ ,  $\mu_{eff}$ , and  $A_\kappa$  [75]. The calculation of the code Vevacious indicated that only about 1% of the scanned samples predict short-lived vacuum.

### 3.2 Numerical results

The discussion begins with the normalized two-dimensional profile likelihood (PL),  $\mathcal{L}(\theta'_1, \theta'_2)$ , for the likelihood function in Eq. (3.2), where  $\mathcal{L}(\theta'_1, \theta'_2)$  is defined as the maximum value of  $\mathcal{L}$  in the position  $\theta_1 = \theta'_1, \theta_2 = \theta'_2$ . In Fig. 1, all of the samples

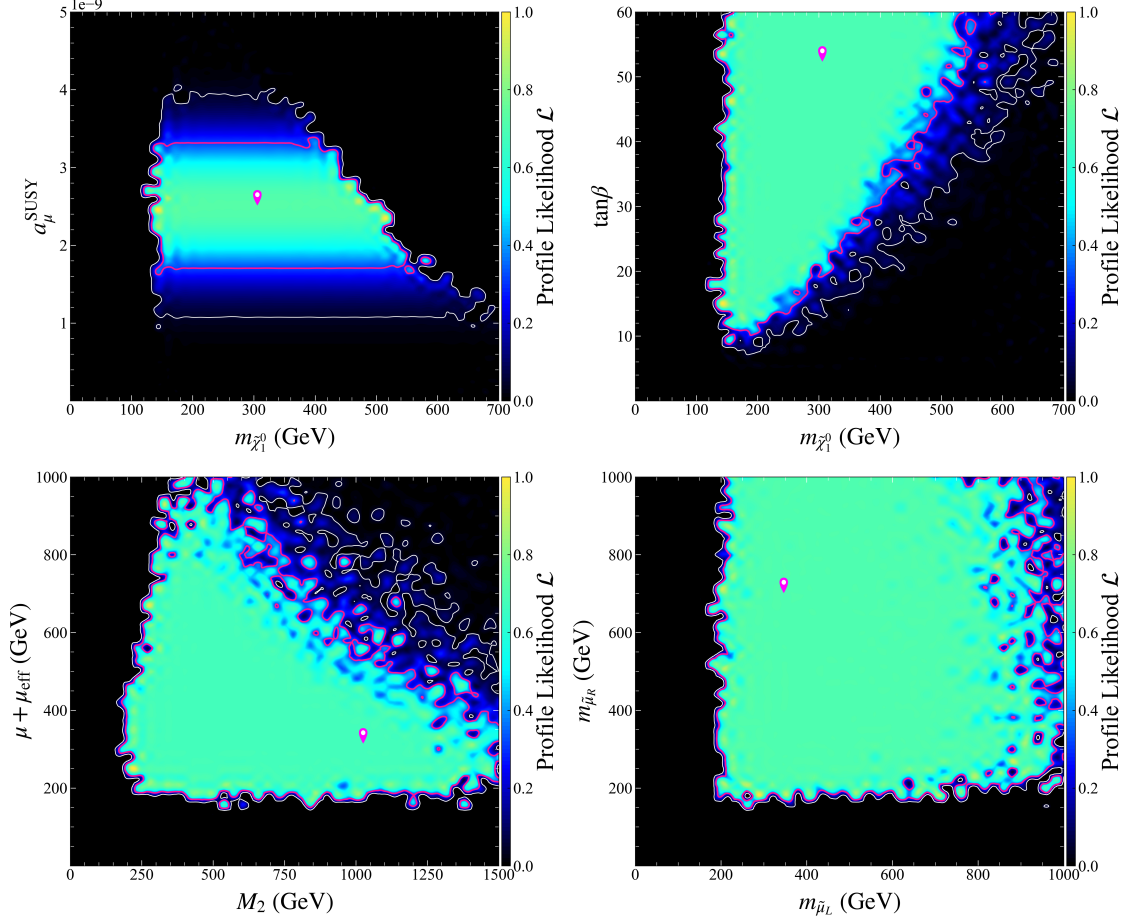


**Figure 1.** Two-dimensional profile likelihood map of the function in Eq. (3.2) projected onto  $m_{\tilde{\chi}_1^0} - a_\mu^{\text{SUSY}}$ ,  $m_{\tilde{\chi}_1^0} - \tan\beta$ ,  $M_2 - (\mu + \mu_{\text{eff}})$ , and  $m_{\tilde{\mu}_L} - m_{\tilde{\mu}_R}$  planes.  $1\sigma$  ( $2\sigma$ ) confidence regions are shown by pink (white) contour lines. The best point locates at  $m_{\tilde{\chi}_1^0} = 305$  GeV,  $\mu + \mu_{\text{eff}} \simeq 340$  GeV,  $M_2 \simeq 1050$  GeV,  $m_{\tilde{\mu}_L} \simeq 350$  GeV, and  $m_{\tilde{\mu}_R} \simeq 740$  GeV, and is marked by the pin symbol. Its  $R$  value defined in Sec. 4 is about 0.3.

are projected onto  $m_{\tilde{\chi}_1^0} - a_\mu^{\text{SUSY}}$ ,  $m_{\tilde{\chi}_1^0} - \tan\beta$ ,  $(\mu + \mu_{\text{eff}}) - M_2$ , and  $m_{\tilde{\mu}_L} - m_{\tilde{\mu}_R}$  planes to obtain the PLs. From Fig. 1, one can find that the  $\mu\text{NMSSM}$  can interpret  $\Delta a_\mu$  in broad parameter space satisfying all of the experimental constraints. The lower mass bounds of particles come from the assumption of  $m_{h_s} \geq 125$  GeV, so the DM masses are often larger than 150 GeV (See the following discussion. A similar result can be found in Fig. 1 of Ref. [74]). The upper bound of the LSP mass  $m_{\tilde{\chi}_1^0}$  is mainly determined by the value of  $\tan\beta$  and  $\Delta a_\mu$ , e.g.,  $a_\mu^{\text{SUSY}} = 2 \times 10^{-9}$  and  $\tan\beta = 60$  set up an upper limit of approximately 550 GeV for  $m_{\tilde{\chi}_1^0}$ . For most samples, the wino-higgsino loop provides the dominant contribution in  $a_\mu^{\text{SUSY}}$ . Within the  $1\sigma$  level in  $\Delta a_\mu$ , the contours in the  $(\mu + \mu_{\text{eff}}) - M_2$  plane imply that the mass of chargino  $\tilde{\chi}_1^\pm$  cannot be larger than approximately 700 GeV (in particular, the higgsino mass may be less than 500 GeV to predict  $m_Z$  naturally), while both  $m_{\tilde{\mu}_L}$  and  $m_{\tilde{\mu}_R}$  can be



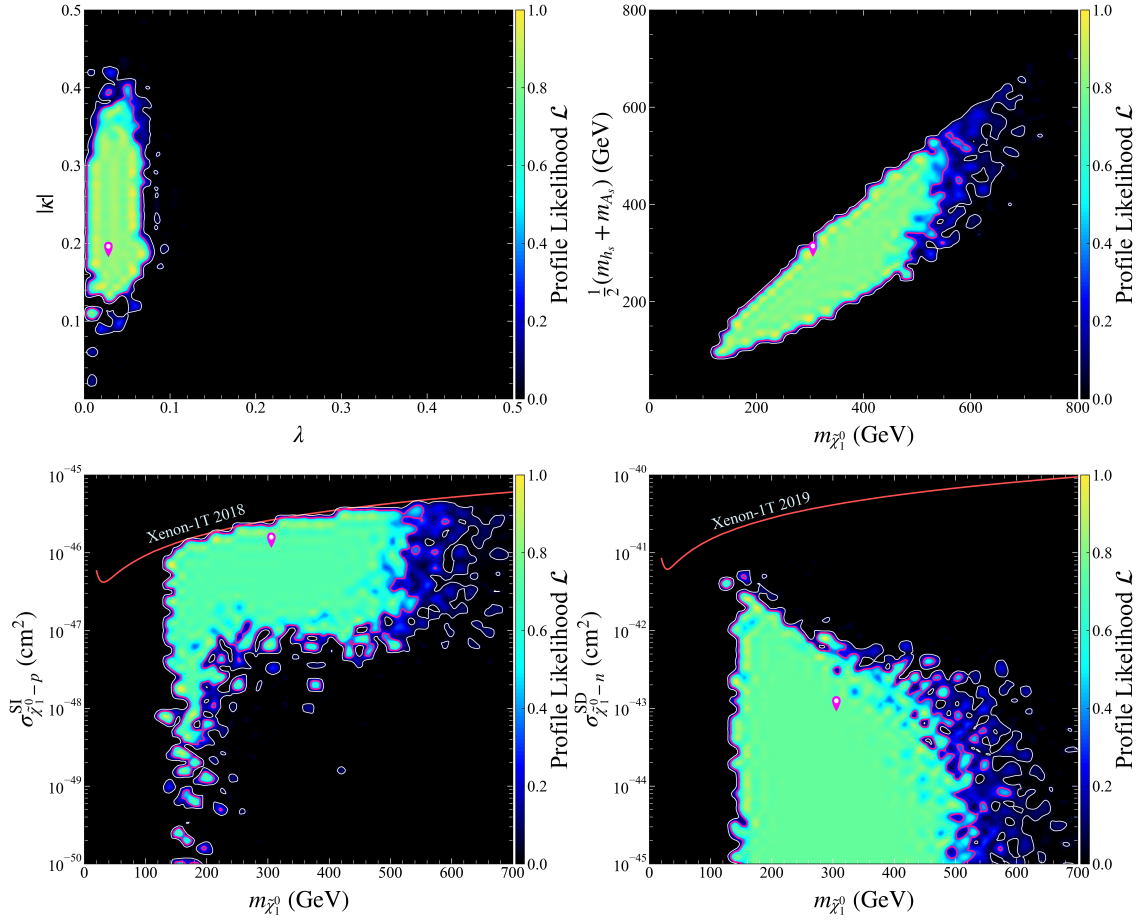


**Figure 2.** Similar to Fig. 1, but onto  $\lambda - |\kappa|$ ,  $m_{\tilde{\chi}_1^0} - \frac{1}{2}(m_{h_s} + m_{A_s})$ ,  $m_{\tilde{\chi}_1^0} - \sigma_n^{\text{SD}}$ , and  $m_{\tilde{\chi}_1^0} - \sigma_p^{\text{SI}}$  planes, respectively.

larger than 800 GeV.

As shown in Fig. 2,  $\lambda$  is less than 0.1, the absolute values of  $\kappa$  vary from 0.1 to 0.4, and all of the samples meet the condition  $m_{\tilde{\chi}_1^0} \gtrsim (m_{h_s} + m_{A_s})/2$ . This feature indicates that the strengths of DM coupled to other non-singlet fields are relatively weak, and the main DM annihilation channel is  $\tilde{\chi}_1^0 \tilde{\chi}_1^0 \rightarrow h_s A_s$ . Thus, the singlet-dominated particles form a secluded DM sector where the singlet Higgs states  $h_s$  and  $A_s$  act as the mediators between DM and SM particles [133], which was pointed out in our previous work [74]. Owing to the smallness of  $\lambda$ , the DM direct detection rates  $\sigma_p^{\text{SI}}$  and  $\sigma_n^{\text{SD}}$  in the  $\Delta a_\mu$  favored parameter space can be far below the current detection limits. **The above discussion shows that the DM phenomenology and natural interpretations of  $\Delta a_\mu$  are very weakly connected in the  $\mu\text{NMSSM}$ .** This situation is significantly different from the MSSM case, where the bino-dominated  $\tilde{\chi}_1^0$  mainly co-annihilated with the other sparticles to obtain the measured relic density, and consequently the parameter space to explain  $\Delta a_\mu$  is limited [46, 47].

In Fig. 3, the mass distributions of the singlet Higgs states and SUSY particles

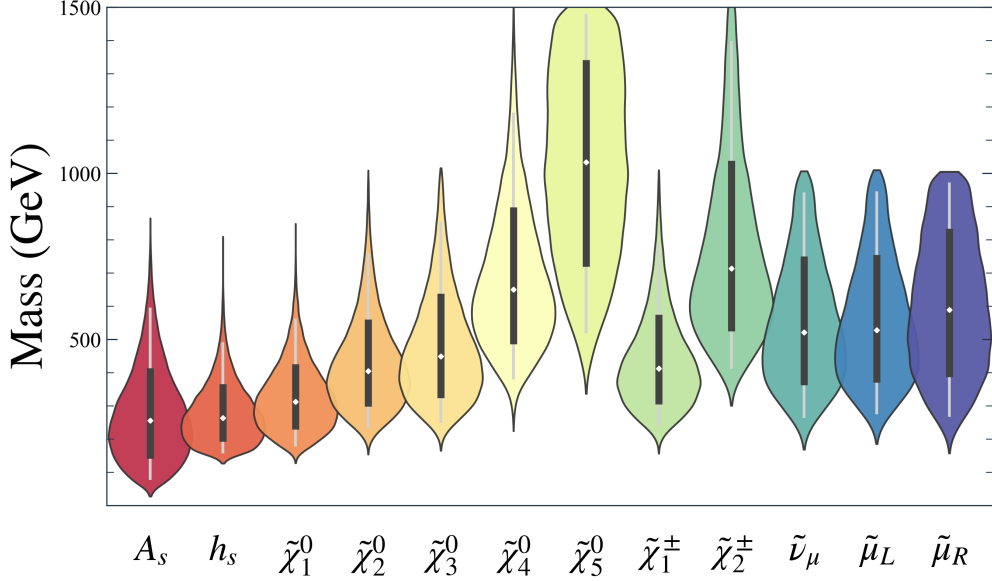


**Figure 3.** Violin plots showing mass distributions of singlet Higgs, EWinos, and  $\mu$ -type sparticles. Smuons are labeled by their dominated components. The violins are scaled by count. Thick vertical bar in center indicates interquartile range with white dot representing the median; long vertical line represents 95% confidence interval.

are shown with violin plots<sup>8</sup>. From Fig. 3, one can find that the masses of sleptons and EWinos can be lower than 500 GeV. They can be produced at the LHC, and they are thus restricted by searching for multi-lepton signals. Compared with the MSSM prediction, the particles in the  $\mu$ NMSSM have the following distinct features.

- As shown in Figs. 1 and 2,  $\tilde{\chi}_1^0$  is moderately massive  $m_{\tilde{\chi}_1^0} > 150$  GeV from the current results because it must be heavier than  $(m_{h_s} + m_{A_s})/2$  to proceed with  $\tilde{\chi}_1^0 \tilde{\chi}_1^0 \rightarrow h_s A_s$ .
- Since  $\tilde{\chi}_1^0$  is singlino-dominated, and thus coupled very weakly to the other sparticles, heavy sparticles prefer to decay into next-to-LSP (NLSP) or next-next-to-LSP (NNLSP) first. Consequently, their decay chain is lengthened and their signals become complicated.
- Since singlet-dominated Higgs bosons are preferred light, they may serve as sparticle decay products and enrich the decay channels of sparticles.

These characteristics make sparticle detection at the LHC rather tricky, and the corresponding constraints should be weaker than those in the simplified models and in the MSSM. This issue will be intensively studied in the following.

<sup>8</sup>A violin plot combines the advantages of the box plot and probability density distribution plot [134].



## 4 LHC constraints

Given that the capability of the **SModelS** package in implementing the LHC constraints is limited by its database and the strict prerequisites to use it, the LHC detection of sparticles is further studied by Monte Carlo event simulations<sup>9</sup>. The following processes are considered in the simulation:

$$\begin{aligned}
pp &\rightarrow \tilde{\chi}_i^0 \tilde{\chi}_j^\pm, & i = 2, 3, 4, 5; & j = 1, 2 \\
pp &\rightarrow \tilde{\chi}_i^\pm \tilde{\chi}_j^\mp, & i = 1, 2; & j = 1, 2 \\
pp &\rightarrow \tilde{\chi}_i^0 \tilde{\chi}_j^0, & i = 2, 3, 4, 5; & j = 2, 3, 4, 5 \\
pp &\rightarrow \tilde{\mu}_i \tilde{\mu}_j, & i = L, R; & j = L, R
\end{aligned} \tag{4.1}$$

The cross-sections at  $\sqrt{s} = 13$  TeV were obtained at the NLO using the package **Prospino2** [135]. The signal events were generated by **MadGraph\_aMC@NLO** [136, 137] with the package **PYTHIA8** [138] for parton showers, hadronization, and sparticle decay. Finally, the event files were put into **CheckMATE-2.0.29** [139–141] with the embedded package **Delphes**[142] for detector simulation.

In the simulations,  $10^5$  signal events were generated for each  $\mu$ NMSSM parameter point, and the following latest LHC searches among the analyses mentioned before were found crucial in testing the samples:

- ATLAS search for chargino and slepton pair production in two lepton final states (see Report No. CERN-EP-2019-106) [143].
- Search for chargino-neutralino production with involved mass splittings near the electroweak scale in three-lepton final states in  $\sqrt{s} = 13$  TeV pp collisions with the ATLAS detector (see Report No. CERN-EP-2019-263) [144].
- Search for direct production of electroweakinos in final states with one lepton, missing transverse momentum and a Higgs boson decaying into two bb jets in pp collisions at  $\sqrt{s} = 13$  TeV with the ATLAS detector (see Report No. CERN-EP-2019-188) [145].
- CMS combined search for charginos and neutralinos (see Report No. CMS-SUS-17-004) [146].
- CMS search for final states with two opposite sign same-flavor leptons, jets, and missing transverse momentum (see Report No. CMS-SUS-20-001) [147].

---

<sup>9</sup>More than 88000 samples were obtained in the previous scan. In order to save time and at the same time make our conclusions as general as possible, a smaller  $n_{\text{live}}$  ( $n_{\text{live}} = 3000$ ) was chosen to repeat the scan and obtained about 7500 samples for studying the LHC constraints. These samples satisfy the vacuum stability requirement and can interpret  $\Delta a_\mu$  within  $2\sigma$  level. Besides, the analyses of  $\sqrt{s} = 8$  TeV pp collisions were not considered in this work because the LSP is relatively heavy so that their constraints on the theory are weak.

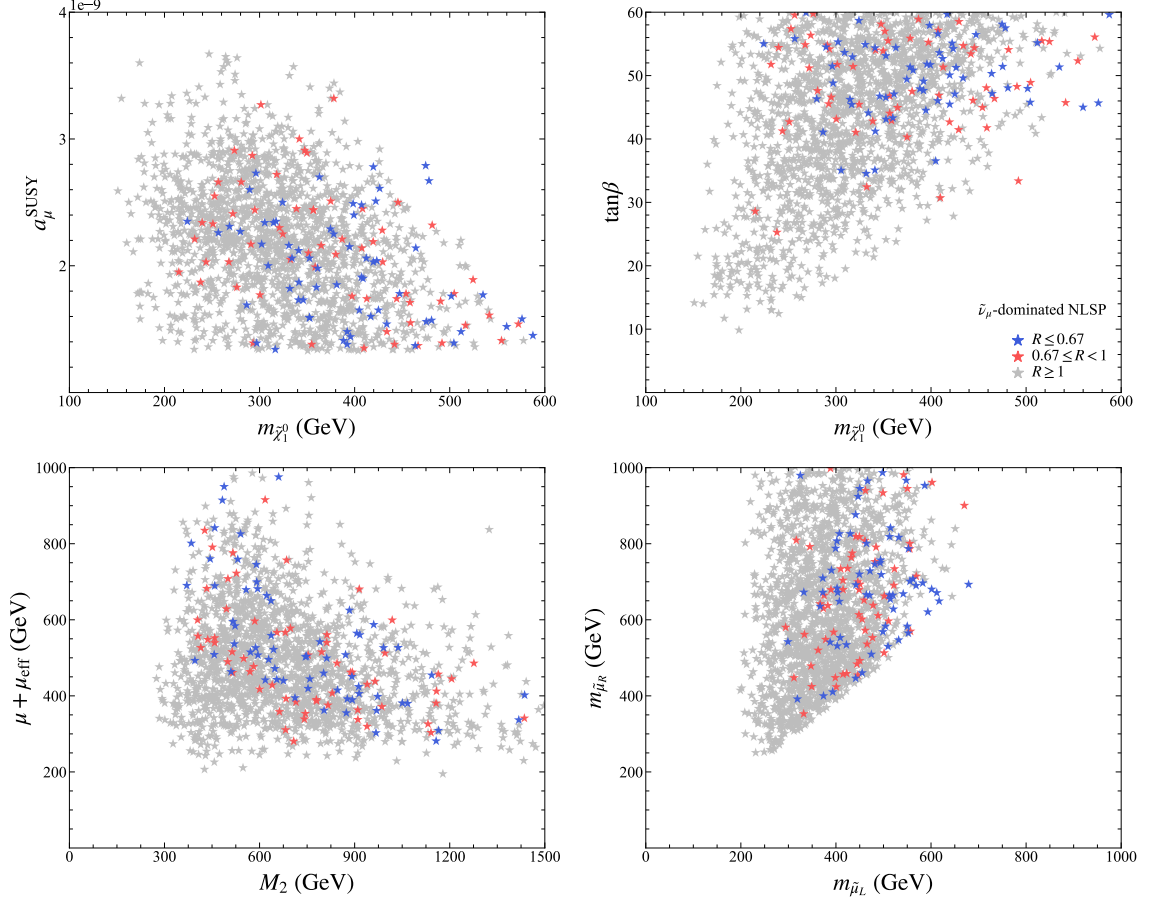


**Figure 4.** The LHC constraints on the samples with  $\tilde{\nu}_\mu$ -dominated NLSP. The samples are projected on  $m_{\tilde{\chi}_1^0} - a_\mu^{\text{SUSY}}$ ,  $m_{\tilde{\chi}_1^0} - \tan\beta$ ,  $M_2 - (\mu + \mu_{\text{eff}})$  and  $m_{\tilde{\mu}_k} - m_{\tilde{\mu}_L}$  planes, and those satisfying  $R \geq 1$ ,  $0.67 \leq R < 1$  and  $R < 0.67$  are marked by grey, red, and blue colors, respectively.

The  $R$  values obtained from the code **CheckMATE** were applied to implement the LHC constraints. Here,  $R \equiv \max\{S_i/S_{\text{obs},i}^{95}\}$  for all the involved analyses, where  $S_i$  represents the simulated event number of the  $i$ th signal region (SR), and  $S_{\text{obs},i}^{95}$  is the corresponding 95% confidence level upper limit. Therefore,  $R > 1$  indicates that the sample is excluded by the LHC searches if the involved uncertainties are not considered (see the discussion in footnote 9 of this work).

The collider simulation results via the **CheckMATE** show that the LHC searches for supersymmetry set clearly limits on the mass spectrum. In order to show details of the results, the samples are classified by their NLSP's dominant component, which may be  $\tilde{\nu}_\mu$ ,  $\tilde{\mu}_R$ ,  $\tilde{B}$ ,  $\tilde{W}$ , or  $\tilde{H}$ . In Figs. 4, 5, and 6, samples featured by  $\tilde{\nu}_\mu$ -,  $\tilde{\mu}_R$ -, and  $\tilde{B}$ -dominated NLSP, respectively, are projected on  $m_{\tilde{\chi}_1^0} - a_\mu^{\text{SUSY}}$  (upper left panel),  $m_{\tilde{\chi}_1^0} - \tan\beta$  (upper right panel),  $M_2 - (\mu + \mu_{\text{eff}})$  (lower left panel) and  $m_{\tilde{\mu}_L} - m_{\tilde{\mu}_R}$  (lower right panel) planes. Most of the samples, which are marked by grey color,

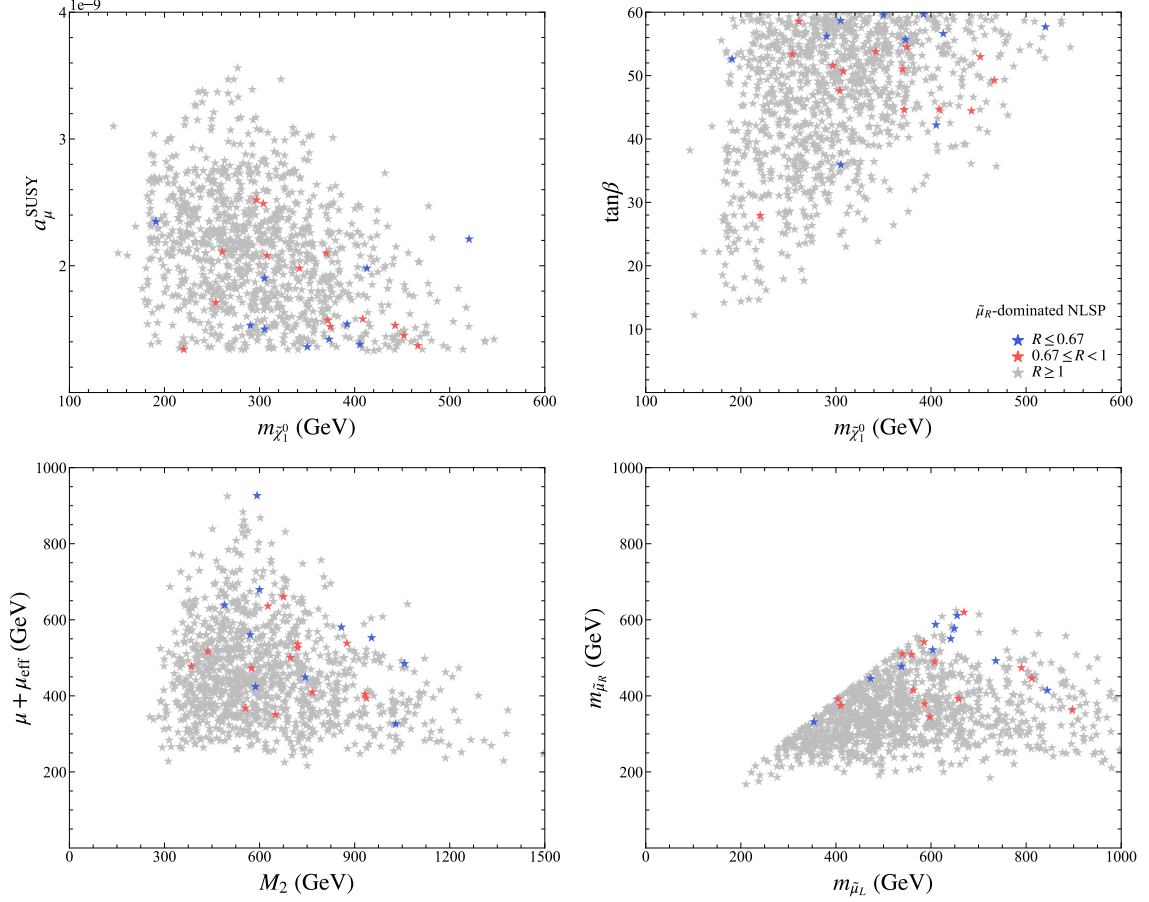


**Figure 5.** Similar to Fig. 4, but for the samples with  $\tilde{\mu}_R$ -dominated NLSP.

NLSP	$m_{\tilde{\chi}_1^0}$	$\mu + \mu_{\text{eff}}$	$M_2$	$m_{\tilde{\mu}_L}$	$m_{\tilde{\mu}_R}$	$N_{\text{tot}}$	$N_{\text{pass}}$
$\tilde{\nu}_\mu$	200	250	370	250	300	1748	124
$\tilde{\mu}_R$	200	300	350	350	300	1071	24
$\tilde{B}$	200	300	300	350	350	310	103
$\tilde{W}$	200	300	250	350	350	1238	784
$\tilde{H}$	160	200	300	250	250	3162	1606

**Table 1.** Summarization of the samples classified by their NLSP's dominant component.  $N_{\text{tot}}$  represents the total number of each type of samples surveyed by specific Monte Carlo simulations.  $N_{\text{pass}}$  represents the corresponding number satisfying  $R < 1$ . The lower limits of parameters ( $\mu + \mu_{\text{eff}}$ ),  $M_2$ ,  $m_{\tilde{\chi}_1^0}$ ,  $m_{\tilde{\mu}_L}$ , and  $m_{\tilde{\mu}_R}$  for the samples surviving the constraints are given in units of GeV in each row.

are excluded by the LHC experiments. The rest points marked by red color and blue color stand for those which survive the LHC experiments with  $0.67 \leq R < 1$  and  $R < 0.67$ , respectively<sup>10</sup>. In Figs. 7 and 8, similar diagrams are plotted for the

<sup>10</sup> $0.67 \leq R < 1$  means that the sample's signal is close to exclusion, but a full accounting of

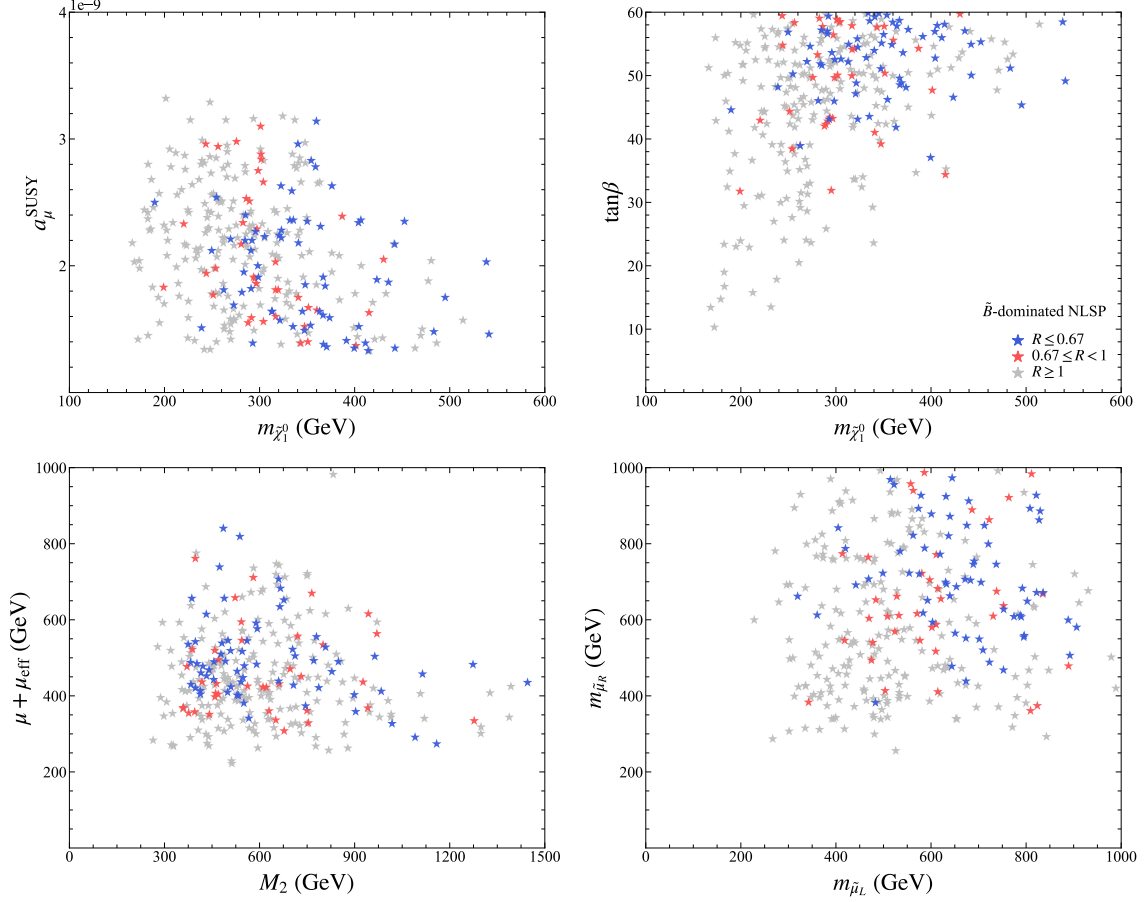


**Figure 6.** Similar to Fig. 4, but for the samples with  $\tilde{B}$ -dominated NLSP.

samples with  $\tilde{W}$ - and  $\tilde{H}$ -dominated NLSP, respectively. The total number of each type of samples surveyed by specific Monte Carlo simulations and the corresponding number satisfying  $R < 1$  are summarized in Table 1, which are denoted by  $N_{\text{tot}}$  and  $N_{\text{pass}}$ , respectively. The lower limits of the representative parameters  $(\mu + \mu_{\text{eff}})$ ,  $M_2$ ,  $m_{\tilde{\chi}_1^0}$ ,  $m_{\tilde{\mu}_L}$  and  $m_{\tilde{\mu}_R}$  after considering the LHC constraints are also presented in the table.

From Figs. 4-8 and Table 1, the following conclusions are inferred:

- Due to the singlet nature of the LSP, sparticle prefers to decay first into lighter sparticles other than the LSP. When  $\tilde{\nu}_\mu$  or  $\tilde{\mu}_R$  acts as NLSP, wino-dominated and higgsino-dominated EWinos decay mostly via slepton and/or sneutrino into leptonic final states, which can enhance the multi-lepton signals. The

---

uncertainties (originating from e.g., parton distribution function sets, the choice of renormalization and factorisation scale, the details of parton showering or the finite Monte Carlo statistics) would certainly place it within error bars [54]. On the other hand, if  $R < 0.67$ , the sample appears to be essentially compatible with the experimental results. It corresponds to the number of signal events which is below the 95% C.L. upper bound divided by 1.5.

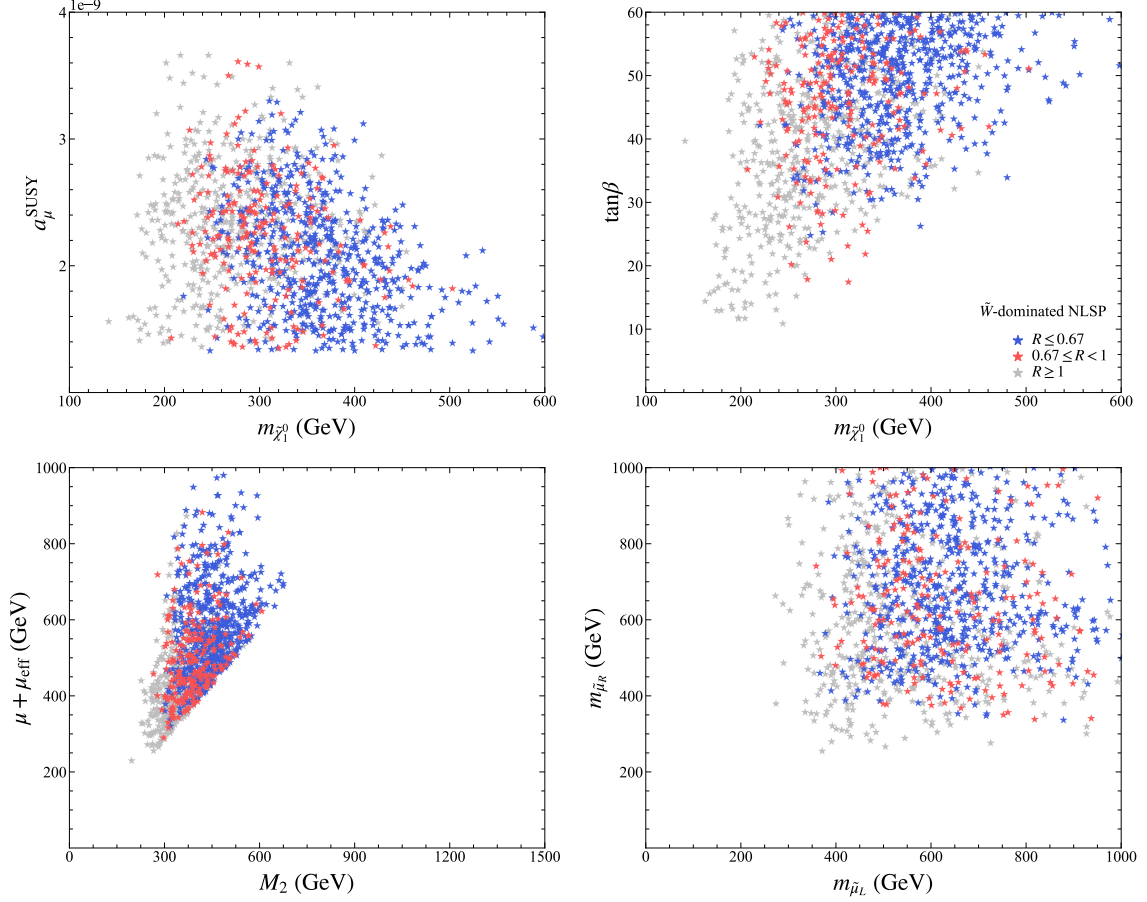


**Figure 7.** Similar to Fig. 4, but for the samples with  $\tilde{W}$ -dominated NLSP.

sparticle's signal is similar to the prediction of the simplified models adopted by ATLAS and CMS collaborations in analyzing experimental data, and it is highly restricted by the current LHC searches.

- When the bino-dominated  $\tilde{\chi}_2^0$  is NLSP, EWinos and sleptons prefer to decay into it with significant branching ratios because  $\tilde{\chi}_2^0$  couples to these particles with unsuppressed gauge interactions. For samples featured by  $\Delta \equiv m_{\tilde{\chi}_2^0} - m_{\tilde{\chi}_1^0}$  less than dozens of GeV,  $\tilde{\chi}_2^0$  appears as a missing track at the collider detector. The signal is similar to the MSSM prediction with a bino-dominated LSP, and it leads to strong constraints on the samples from the LHC searches for supersymmetry. However,  $\tilde{\chi}_2^0$  will decay by  $\tilde{\chi}_2^0 \rightarrow \tilde{\chi}_1^0 h$ ,  $\tilde{\chi}_1^0 Z$  if  $\Delta > m_h$ , and the  $\tilde{\chi}_1^0 h$  channel is usually dominant. In this case, it is hard to detect the sparticles partially due to the complexity of the decay chain.
- For samples with wino- or higgsino-dominated  $\tilde{\chi}_2^0$  acting as NLSP, the collider constraints are relatively weak. This observation comes from at least three facts. First, since the wino- or higgsino-dominated  $\tilde{\chi}_2^0$  can not decay into slep-

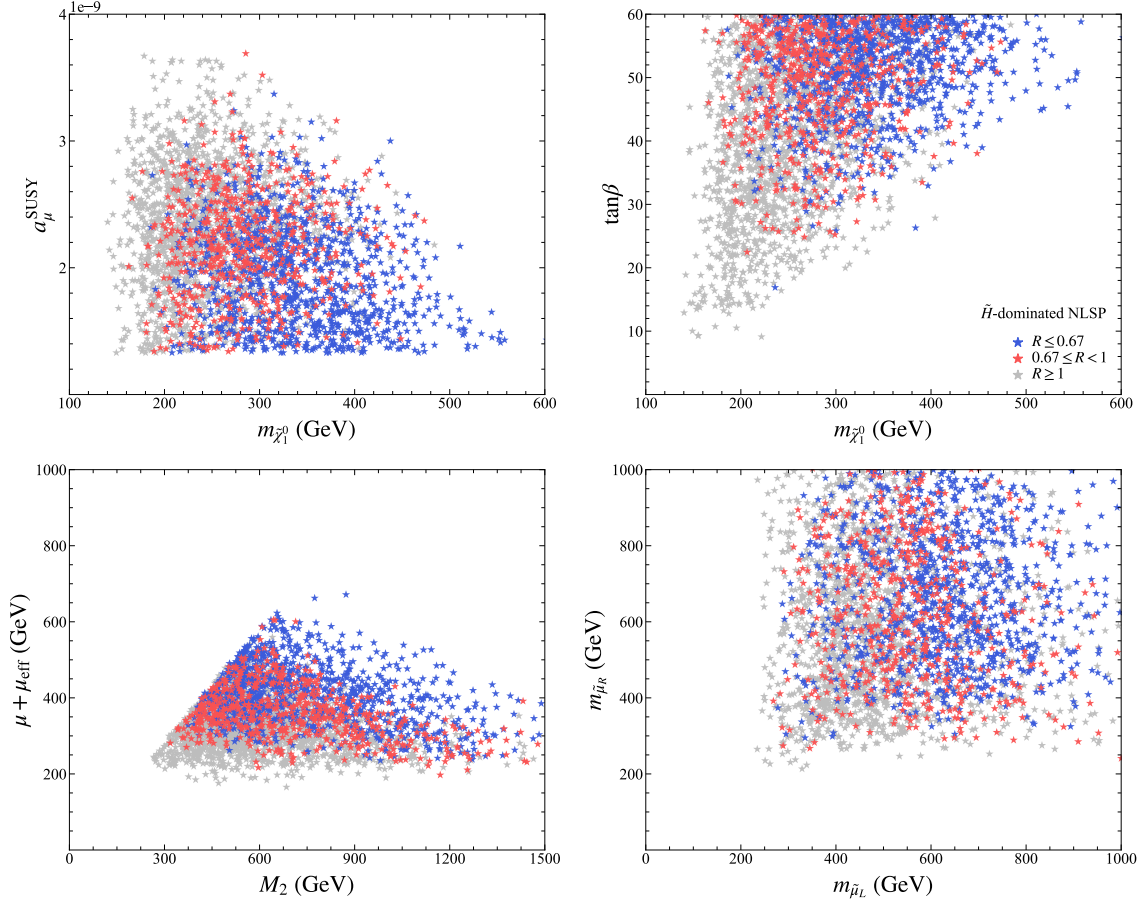


**Figure 8.** Similar to Fig. 4, but for the samples with  $\tilde{H}$ -dominated NLSP.

tons, the leptonic signal rate is usually much smaller than the case where  $\tilde{\nu}_\mu$  or  $\tilde{\mu}_R$  acts as NLSP. Second, the collider sensitive signal events are often diluted by the complicated decay chains of sparticles given that heavy sparticles prefer to decay into the NLSP first. Third, the interpretation of  $\Delta a_\mu$  requires that EWinos and smuons are in several hundred GeVs. So for most of the samples surviving the LHC constraints, the mass splitting between sparticles is not large enough to produce high- $p_T$  signal objects which can be significantly distinguished from the background in the collider. For example, it was found that the samples featured by wino-dominated NLSP receive the weakest restriction, and most of the surviving samples roughly satisfy  $m_{\tilde{\chi}_1^0} \gtrsim 200$  GeV,  $M_2 - m_{\tilde{\chi}_1^0} \lesssim 150$  GeV and  $(\mu + \mu_{\text{eff}}) - M_2 \lesssim 200$  GeV. This parameter configuration is not sensitive to the current LHC EWino direct searches (see, e.g., point P2 in Table 2).

In addition, it is noticeable that most of the surviving samples are characterized by  $\mu + \mu_{\text{tot}} < 600$  GeV, which can predict  $m_Z$  naturally. It is a distinct difference between the  $\mu$ NMSSM and MSSM.



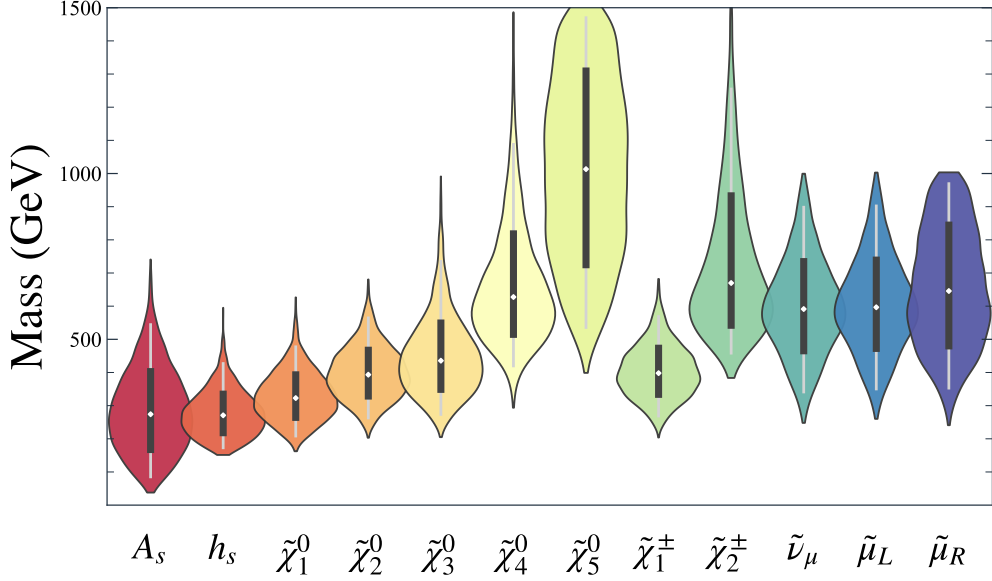


**Figure 9.** Same as Fig. 3, but for the samples surviving the LHC constraints.

- The  $a_\mu^{\text{SUSY}}$  enhancement factor  $\tan\beta$  is apparently restricted by the current LHC constraints. As indicated by the upper right panel of Figs. 4-8, the LHC observations require  $\tan\beta$  larger than about 20 to interpret  $\Delta a_\mu$  within  $2\sigma$  level, and about 30 within  $1\sigma$  level.
- It should be noted that some of the latest LHC analyses, e.g., the analysis in [148], are not included in this work. However, one can make some rough estimations by thinking that the red points in Figs. 4-8 will be excluded by the latest or the near future LHC analyses. There is still a relatively large parameter space of the  $\mu\text{NMSSM}$  that can interpret  $\Delta a_\mu$  without conflicting with the newest LHC analyses. So the LHC constraints considered in this article are of a reference value.

In order to emphasize the properties of the samples with higgsino-dominated  $\tilde{\chi}_2^0$  and wino-dominated  $\tilde{\chi}_2^0$ , two benchmark points, P1 and P2, are chosen to present their detailed information in Table 2. Both points predict  $a_\mu^{\text{SUSY}}$  values approximately equal to  $2.51 \times 10^{-9}$  and pass all the experimental constraints. These two benchmark points verify our previous discussions.

Finally, the mass spectra of the sparticles surviving the LHC constraints are presented in Fig. 9. Comparing it with Fig. 3, it was found that the LHC constraints are very effective in excluding relatively light sparticles, especially light sleptons. In fact, this conclusion is also reflected in the last three panels of Figs. 4-8. Another important conclusion is that the  $\tilde{W}$  or  $\tilde{H}$ -dominated  $\tilde{\chi}_1^\pm$  is always lighter than about 700 GeV. Taking into account its production cross-section at linear  $e^+e^-$  collid-

Benchmark Point P1				Benchmark Point P2			
$\lambda$	0.019	$m_{h_s}$	364.4 GeV	$\lambda$	0.017	$m_{h_s}$	233.1 GeV
$\kappa$	-0.267	$m_{A_s}$	262.1 GeV	$\kappa$	0.234	$m_{A_s}$	315.8 GeV
$\tan \beta$	54.99	$m_h$	125.5 GeV	$\tan \beta$	59.87	$m_h$	124.7 GeV
$\mu$	423.3 GeV	$m_H$	1970 GeV	$\mu$	640.6 GeV	$m_H$	2388 GeV
$\mu + \mu_{\text{eff}}$	437.6 GeV	$m_{A_H}$	1970 GeV	$\mu + \mu_{\text{eff}}$	651.4 GeV	$m_{A_H}$	2388 GeV
$A_t$	2545 GeV	$m_{\tilde{\chi}_1^0}$	394.5 GeV	$A_t$	2570 GeV	$m_{\tilde{\chi}_1^0}$	295.2 GeV
$A_\kappa$	116.6 GeV	$m_{\tilde{\chi}_2^0}$	425.9 GeV	$A_\kappa$	-225.9 GeV	$m_{\tilde{\chi}_2^0}$	445.2 GeV
$M_1$	1086 GeV	$m_{\tilde{\chi}_3^0}$	452.6 GeV	$M_1$	-1239 GeV	$m_{\tilde{\chi}_3^0}$	665.7 GeV
$M_2$	541.7 GeV	$m_{\tilde{\chi}_4^0}$	591.0 GeV	$M_2$	443.0 GeV	$m_{\tilde{\chi}_4^0}$	679.9 GeV
$m_L$	609.6 GeV	$m_{\tilde{\chi}_5^0}$	1091 GeV	$m_L$	539.5 GeV	$m_{\tilde{\chi}_5^0}$	1244 GeV
$m_E$	992.4 GeV	$m_{\tilde{\chi}_1^\pm}$	429.9 GeV	$m_E$	697.9 GeV	$m_{\tilde{\chi}_1^\pm}$	445.5 GeV
$a_\mu^{\text{SUSY}}$	$2.514 \times 10^{-9}$	$m_{\tilde{\chi}_2^\pm}$	592.0 GeV	$a_\mu^{\text{SUSY}}$	$2.510 \times 10^{-9}$	$m_{\tilde{\chi}_2^\pm}$	682.2 GeV
$\Omega h^2$	0.142	$m_{\tilde{\mu}_L}$	617.5 GeV	$\Omega h^2$	0.108	$m_{\tilde{\mu}_L}$	546.3 GeV
$\sigma_p^{\text{SI}}$	$2.02 \times 10^{-47} \text{ cm}^2$	$m_{\tilde{\mu}_R}$	927.3 GeV	$\sigma_p^{\text{SI}}$	$1.47 \times 10^{-46} \text{ cm}^2$	$m_{\tilde{\mu}_R}$	793.8 GeV
$\sigma_n^{\text{SD}}$	$1.84 \times 10^{-45} \text{ cm}^2$	$m_{\tilde{\nu}_\mu}$	612.0 GeV	$\sigma_n^{\text{SD}}$	$1.83 \times 10^{-47} \text{ cm}^2$	$m_{\tilde{\nu}_\mu}$	540.3 GeV
$N_{11}, N_{12}, N_{13}, N_{14}, N_{15}$	0.000, 0.002, 0.027, 0.031, -0.999			$N_{11}, N_{12}, N_{13}, N_{14}, N_{15}$	0.000, 0.003, -0.003, 0.006, 0.999		
$N_{21}, N_{22}, N_{23}, N_{24}, N_{25}$	0.043, -0.365, 0.674, -0.640, -0.003			$N_{21}, N_{22}, N_{23}, N_{24}, N_{25}$	-0.004, -0.969, 0.206, -0.138, -0.004		
$N_{31}, N_{32}, N_{33}, N_{34}, N_{35}$	-0.020, 0.054, 0.703, 0.708, 0.041			$N_{31}, N_{32}, N_{33}, N_{34}, N_{35}$	-0.053, 0.049, -0.705, -0.705, -0.002		
$N_{41}, N_{42}, N_{43}, N_{44}, N_{45}$	0.026, 0.929, 0.224, -0.293, -0.001			$N_{41}, N_{42}, N_{43}, N_{44}, N_{45}$	0.016, -0.242, -0.678, 0.693, 0.005		
$N_{51}, N_{52}, N_{53}, N_{54}, N_{55}$	0.999, -0.007, -0.021, 0.049, 0.000			$N_{51}, N_{52}, N_{53}, N_{54}, N_{55}$	0.998, -0.002, -0.025, -0.049, 0.000		
Annihilations		Fractions [%]		Annihilations		Fractions [%]	
$\tilde{\chi}_1^0 \tilde{\chi}_1^0 \rightarrow h_s A_s / h_s h_s / \dots$		78.7 / 4.1 / ...		$\tilde{\chi}_1^0 \tilde{\chi}_1^0 \rightarrow h_s A_s / h_s h_s / h A_s$		94.5 / 4.4 / 1.1	
Decays		Branching ratios [%]		Decays		Branching ratios [%]	
$\tilde{\chi}_2^0 \rightarrow \tilde{\chi}_1^0 Z^* (\rightarrow \tilde{\chi}_1^0 f \bar{f})$		100		$\tilde{\chi}_2^0 \rightarrow \tilde{\chi}_1^0 h / \tilde{\chi}_1^0 Z$		99.8 / 0.2	
$\tilde{\chi}_3^0 \rightarrow \tilde{\chi}_1^0 Z^* (\rightarrow \tilde{\chi}_1^0 f \bar{f}) / \tilde{\chi}_1^\pm W^\mp (\rightarrow \tilde{\chi}_1^\pm f \bar{f})$		46.3 / 53.6		$\tilde{\chi}_3^0 \rightarrow \tilde{\chi}_1^\pm W^\mp / \tilde{\chi}_2^0 Z$		68.3 / 30.3	
$\tilde{\chi}_4^0 \rightarrow \tilde{\chi}_1^\pm W^\mp / \tilde{\chi}_3^0 Z / \tilde{\chi}_3^0 h$		70.0 / 15.1 / 14.0		$\tilde{\chi}_4^0 \rightarrow \tilde{\chi}_1^\pm W^\mp / \tilde{\chi}_2^0 h / \tilde{\chi}_2^0 Z$		69.2 / 27.5 / 1.6	
$\tilde{\chi}_5^0 \rightarrow \tilde{\chi}_1^\pm W^\mp / \tilde{\chi}_{2,3}^0 Z / \tilde{\chi}_{2,3}^0 h / \tilde{\mu}_L \mu / \tilde{\nu}_\mu \nu_\mu$		21.2 / 14.7 / 12.1 / 29.8 / 9.9		$\tilde{\chi}_5^0 \rightarrow \tilde{\mu}_L \mu / \tilde{\mu}_R \mu / \tilde{\nu}_\mu \nu_\mu / \tilde{\chi}_2^\pm W^\mp / \tilde{\chi}_3^0 h$		13.3 / 38.1 / 13.7 / 15.3 / 8.1	
$\tilde{\chi}_1^\pm \rightarrow \tilde{\chi}_1^0 W^*$		100		$\tilde{\chi}_1^\pm \rightarrow \tilde{\chi}_1^0 W^\pm$		100	
$\tilde{\chi}_2^\pm \rightarrow \tilde{\chi}_{2,3}^0 W^\pm / \tilde{\chi}_1^\pm Z$		55 / 23		$\tilde{\chi}_2^\pm \rightarrow \tilde{\chi}_3^0 W^\pm / \tilde{\chi}_1^\pm h / \tilde{\chi}_1^\pm Z / \tilde{\mu}_L \nu_\mu$		36.1 / 33.5 / 28.5 / 1.1	
$\tilde{\mu}_L \rightarrow \tilde{\chi}_1^\pm \nu_\mu / \tilde{\chi}_2^0 \mu / \tilde{\chi}_2^0 \nu_\mu / \tilde{\chi}_3^0 \mu$		52.0 / 30.4 / 10.8 / 5.8		$\tilde{\mu}_L \rightarrow \tilde{\chi}_1^\pm \nu_\mu / \tilde{\chi}_2^0 \mu$		65.9 / 34.1	
$\tilde{\mu}_R \rightarrow \tilde{\chi}_{2,3}^0 \mu / \tilde{\chi}_1^\pm \nu_\mu / \tilde{\mu}_L h / \tilde{\mu}_L Z / \tilde{\nu}_\mu W^-$		48.3 / 29.9 / 3.3 / 3.2 / 7.0		$\tilde{\mu}_R \rightarrow \tilde{\nu}_\mu W^- / \tilde{\mu}_L h / \tilde{\mu}_L Z / \tilde{\chi}_3^0 \mu$		54.0 / 21.8 / 19.8 / 2.2	
$\tilde{\nu}_\mu \rightarrow \tilde{\chi}_1^\pm \mu / \tilde{\chi}_2^0 \nu_\mu / \tilde{\chi}_3^0 \mu / \tilde{\chi}_3^0 \nu_\mu$		64.5 / 27.7 / 4.6 / 2.6		$\tilde{\nu}_\mu \rightarrow \tilde{\chi}_2^0 \nu_\mu / \tilde{\chi}_1^\pm \mu$		32.8 / 67.2	
$R$ value		0.207		$R$ value		0.393	

**Table 2.** Detailed information of two benchmark points that agree well with all of the DM and Higgs experiments and predict  $a_\mu^{\text{SUSY}} \simeq 2.51 \times 10^{-9}$ . Numbers after annihilation processes represent their fractions in contributing to total DM annihilation cross-section at freeze-out temperature. Numbers after sparticle decay channels denote their branching ratios.

ers [149], one can infer that  $\tilde{\chi}_1^\pm$  is very likely to be discovered at the CLIC, whose collision energy can reach 3 TeV [150–153]. This point was recently emphasized by the authors of [46, 47]. Moreover, as mentioned in [96, 154], future high luminosity LHC can significantly extend the LHC Run-II’s capability in sparticle detection. The preliminary analyses carried out in, e.g., [155–157], have proven this point. These machines provide an opportunity to test the  $\mu\text{NMSSM}$  interpretation of  $\Delta a_\mu$  once the deviation of  $a_\mu^{\text{exp}}$  from the SM prediction is confirmed. This issue will be studied in detail in our future work.

## 5 Summary

In this work, the phenomenology of the new Fermilab result of  $\Delta a_\mu$  interpreted in the  $\mu\text{NMSSM}$  was investigated. The obtained results show the following features:

- Compared with the MSSM or the  $\mathbb{Z}_3\text{-NMSSM}$ , the strong exclusivity from DM physics and natural interpretations of  $\Delta a_\mu$  is weak in the  $\mu\text{NMSSM}$ .



- A singlino-dominated DM candidate is preferred in the interpretation. Owing to the smallness of the singlet-doublet Higgs coupling  $\lambda$ , the singlino-dominated neutralino and singlet-dominated Higgs bosons may form a secluded DM sector in which the annihilation channel  $\tilde{\chi}_1^0 \tilde{\chi}_1^0 \rightarrow h_s A_s$  is responsible for the measured abundance by adopting an appropriate singlet Yukawa coupling  $\kappa$ .
- The secluded sector communicates with the SM sector by weak singlet-doublet Higgs mixing, so the scatterings of singlino-dominated DM with nucleons are suppressed below the current experimental limits.
- The mass of DM  $m_{\tilde{\chi}_1^0}$  must be heavier than about 150 GeV to proceed with the annihilation, and must be lighter than about 550 GeV to explain  $\Delta a_\mu$  at  $1\sigma$  level.
- Owing to the singlet nature of DM and the complex mass hierarchy of sparticles, the decay chains of EWinos and sleptons are lengthened in comparison with the MSSM prediction. Moreover, the singlet Higgs bosons  $h_s$  and  $A_s$  in the final states of the searching channels weaken the LHC detection capability. These characteristics make particle detection at the LHC rather tricky.

This study shows that the proposed theory can readily explain the discrepancy of the muon anomalous magnetic moment between its SM prediction and experimentally measured value, without conflicting with DM and Higgs experimental results and the LHC searches for supersymmetry. Among the interpretations, it is remarkable that the higgsino mass is less than 500 GeV in most cases so that the  $Z$  boson mass can be naturally predicted.

## A Fast simulation via SModelS

**SModelS** [124, 166–170] enables the fast interpretation of the LHC data via simplified model results from ATLAS and CMS searches for SUSY particles. It decomposes all of the signatures occurring in a given SUSY model into simplified model topologies<sup>11</sup> via a generic procedure. In practice, the cross-section upper limits and efficiency maps are used in re-interpreting each topology result. Compared with Monte Carlo simulation, **SModelS** is much easier and faster. It not only allows for re-interpreting searches of the cut-and-count methodology, but it also allows for other searches, such as those relying on boosted decision tree (BDT) variables. The power of **SModelS** comes from its superfast speed and its large and continuously updated database. The

---

<sup>11</sup>Simplified model topologies are also referred to as simplified model spectra. An event topology is defined by the vertex structure as well as the SM and BSM final states. In each topology, the intermediate  $Z_2$  odd BSM particles are characterized only by their masses, production rates, and decay modes.

Analysis	Simplified Scenario	Signal of Final State	Luminosity
CMS-SUS-17-010 [158] (arXiv:1807.07799)	$\tilde{\chi}_1^\pm \tilde{\chi}_1^\mp \rightarrow W^\pm \tilde{\chi}_1^0 W^\mp \tilde{\chi}_1^0$ $\tilde{\chi}_1^\pm \tilde{\chi}_1^\mp \rightarrow \nu \tilde{\ell} / \ell \tilde{\nu} \rightarrow \ell \nu \nu \tilde{\chi}_1^0 \tilde{\chi}_1^0$	$2\ell + E_T^{\text{miss}}$	$35.9 \text{ fb}^{-1}$
CMS-SUS-17-009 [159] (arXiv:1806.05264)	$\tilde{\ell} \tilde{\ell} \rightarrow \ell \ell \tilde{\chi}_1^0 \tilde{\chi}_1^0$	$2\ell + E_T^{\text{miss}}$	$35.9 \text{ fb}^{-1}$
CMS-SUS-17-004 [146] (arXiv:1801.03957)	$\tilde{\chi}_2^0 \tilde{\chi}_1^\pm \rightarrow Wh(Z) \tilde{\chi}_1^0 \tilde{\chi}_1^0$	$n\ell(\geq 0) + nj(\geq 0) + E_T^{\text{miss}}$	$35.9 \text{ fb}^{-1}$
CMS-SUS-16-045 [160] (arXiv:1709.00384)	$\tilde{\chi}_2^0 \tilde{\chi}_1^\pm \rightarrow W^\pm \tilde{\chi}_1^0 h \tilde{\chi}_1^0$	$1\ell 2b + E_T^{\text{miss}}$	$35.9 \text{ fb}^{-1}$
CMS-SUS-16-039 [161] (arxiv:1709.05406)	$\tilde{\chi}_2^0 \tilde{\chi}_1^\pm \rightarrow \ell \tilde{\nu} \tilde{\ell}$ $\tilde{\chi}_2^0 \tilde{\chi}_1^\pm \rightarrow \tilde{\tau} \nu \tilde{\ell}$ $\tilde{\chi}_2^0 \tilde{\chi}_1^\pm \rightarrow \tilde{\tau} \nu \tilde{\tau}$ $\tilde{\chi}_2^0 \tilde{\chi}_1^\pm \rightarrow WZ \tilde{\chi}_1^0 \tilde{\chi}_1^0$ $\tilde{\chi}_2^0 \tilde{\chi}_1^\pm \rightarrow WH \tilde{\chi}_1^0 \tilde{\chi}_1^0$	$n\ell(\geq 0)(\tau) + E_T^{\text{miss}}$	$35.9 \text{ fb}^{-1}$
CMS-SUS-16-034 [162] (arXiv:1709.08908)	$\tilde{\chi}_2^0 \tilde{\chi}_1^\pm \rightarrow W \tilde{\chi}_1^0 Z(h) \tilde{\chi}_1^0$	$n\ell(\geq 2) + nj(\geq 1) E_T^{\text{miss}}$	$35.9 \text{ fb}^{-1}$
CERN-EP-2017-303 [163] (arXiv:1803.02762)	$\tilde{\chi}_2^0 \tilde{\chi}_1^\pm \rightarrow WZ \tilde{\chi}_1^0 \tilde{\chi}_1^0$ $\tilde{\chi}_2^0 \tilde{\chi}_1^\pm \rightarrow \nu \tilde{\ell} \tilde{\ell}$ $\tilde{\chi}_1^\pm \tilde{\chi}_1^\mp \rightarrow \nu \tilde{\ell} / \ell \tilde{\nu} \rightarrow \ell \nu \nu \tilde{\chi}_1^0 \tilde{\chi}_1^0$ $\tilde{\ell} \tilde{\ell} \rightarrow \ell \ell \tilde{\chi}_1^0 \tilde{\chi}_1^0$	$n\ell(\geq 2) + E_T^{\text{miss}}$	$35.9 \text{ fb}^{-1}$
CERN-EP-2018-306 [164] (arXiv:1812.09432)	$\tilde{\chi}_2^0 \tilde{\chi}_1^\pm \rightarrow Wh \tilde{\chi}_1^0 \tilde{\chi}_1^0$	$n\ell(\geq 0) + nj(\geq 0) + nb(\geq 0) + n\gamma(\geq 0) + E_T^{\text{miss}}$	$35.9 \text{ fb}^{-1}$
CERN-EP-2018-113 [165] (arXiv:1806.02293)	$\tilde{\chi}_2^0 \tilde{\chi}_1^\pm \rightarrow WZ \tilde{\chi}_1^0 \tilde{\chi}_1^0$	$n\ell(\geq 2) + nj(\geq 0) + E_T^{\text{miss}}$	$35.9 \text{ fb}^{-1}$
CERN-EP-2019-263 [144] (arXiv:1912.08479)	$\tilde{\chi}_2^0 \tilde{\chi}_1^\pm \rightarrow W \tilde{\chi}_1^0 Z \tilde{\chi}_1^0 \rightarrow \ell \nu \ell \ell \tilde{\chi}_1^0 \tilde{\chi}_1^0$	$3\ell + E_T^{\text{miss}}$	$139 \text{ fb}^{-1}$
CERN-EP-2019-106 [143] (arXiv:1908.08215)	$\tilde{\ell} \tilde{\ell} \rightarrow \ell \ell \tilde{\chi}_1^0 \tilde{\chi}_1^0$ $\tilde{\chi}_1^\pm \tilde{\chi}_1^\mp \rightarrow \nu \tilde{\ell} / \ell \tilde{\nu} \rightarrow \ell \nu \nu \tilde{\chi}_1^0 \tilde{\chi}_1^0$	$2\ell + E_T^{\text{miss}}$	$139 \text{ fb}^{-1}$
CERN-EP-2019-188 [145] (arXiv:1909.09226)	$\tilde{\chi}_2^0 \tilde{\chi}_1^\pm \rightarrow Wh \tilde{\chi}_1^0 \tilde{\chi}_1^0$	$1\ell + h(\rightarrow bb) + E_T^{\text{miss}}$	$139 \text{ fb}^{-1}$
CMS-SUS-20-001 [147] (arXiv:2012.08600)	$\tilde{\chi}_2^0 \tilde{\chi}_1^\mp \rightarrow Z \tilde{\chi}_1^0 W^\mp \tilde{\chi}_1^0$ $\tilde{\ell} \tilde{\ell} \rightarrow \ell \ell \tilde{\chi}_1^0 \tilde{\chi}_1^0$	$2\ell + E_T^{\text{miss}}$	$137 \text{ fb}^{-1}$

**Table 3.** Signal of final state for electroweakino pair-production processes considered in this work. Relevant experimental analyses were performed in simplified models by ATLAS and CMS collaborations, and their results have been encoded in **SModelS-1.2.3**.

applicability of **SModelS** is limited by the simplified model results available in the database. Moreover, when the tested spectra split into many different channels, as is often the case in a complex model, the derived results are generally conservative.

In this work, the samples are refined with the analyses at 13 TeV LHC in **SModelS**, which are summarized in Table 3.

## References

- [1] MUON  $g - 2$  collaboration, B. Abi, T. Albahri, S. Al-Kilani, D. Allspach, L. P. Alonzi, A. Anastasi et al., *Measurement of the positive muon anomalous magnetic moment to 0.46 ppm*, *Phys. Rev. Lett.* **126** (2021) 141801.

- [2] MUON G-2 collaboration, G. W. Bennett et al., *Final Report of the Muon E821 Anomalous Magnetic Moment Measurement at BNL*, *Phys. Rev. D* **73** (2006) 072003 [[hep-ex/0602035](#)].
- [3] T. Aoyama et al., *The anomalous magnetic moment of the muon in the Standard Model*, *Phys. Rept.* **887** (2020) 1 [[2006.04822](#)].
- [4] T. Aoyama, M. Hayakawa, T. Kinoshita and M. Nio, *Complete Tenth-Order QED Contribution to the Muon  $g - 2$* , *Phys. Rev. Lett.* **109** (2012) 111808 [[1205.5370](#)].
- [5] T. Aoyama, T. Kinoshita and M. Nio, *Theory of the Anomalous Magnetic Moment of the Electron*, *Atoms* **7** (2019) 28.
- [6] A. Czarnecki, W. J. Marciano and A. Vainshtein, *Refinements in electroweak contributions to the muon anomalous magnetic moment*, *Phys. Rev.* **D67** (2003) 073006 [[hep-ph/0212229](#)].
- [7] C. Gnendiger, D. Stöckinger and H. Stöckinger-Kim, *The electroweak contributions to  $(g - 2)_\mu$  after the Higgs boson mass measurement*, *Phys. Rev.* **D88** (2013) 053005 [[1306.5546](#)].
- [8] M. Davier, A. Hoecker, B. Malaescu and Z. Zhang, *Reevaluation of the hadronic vacuum polarisation contributions to the Standard Model predictions of the muon  $g - 2$  and  $\alpha(m_Z^2)$  using newest hadronic cross-section data*, *Eur. Phys. J.* **C77** (2017) 827 [[1706.09436](#)].
- [9] A. Keshavarzi, D. Nomura and T. Teubner, *Muon  $g - 2$  and  $\alpha(M_Z^2)$ : a new data-based analysis*, *Phys. Rev.* **D97** (2018) 114025 [[1802.02995](#)].
- [10] G. Colangelo, M. Hoferichter and P. Stoffer, *Two-pion contribution to hadronic vacuum polarization*, *JHEP* **02** (2019) 006 [[1810.00007](#)].
- [11] M. Hoferichter, B.-L. Hoid and B. Kubis, *Three-pion contribution to hadronic vacuum polarization*, *JHEP* **08** (2019) 137 [[1907.01556](#)].
- [12] M. Davier, A. Hoecker, B. Malaescu and Z. Zhang, *A new evaluation of the hadronic vacuum polarisation contributions to the muon anomalous magnetic moment and to  $\alpha(m_Z^2)$* , *Eur. Phys. J.* **C80** (2020) 241 [[1908.00921](#)].
- [13] A. Keshavarzi, D. Nomura and T. Teubner, *The  $g - 2$  of charged leptons,  $\alpha(M_Z^2)$  and the hyperfine splitting of muonium*, *Phys. Rev.* **D101** (2020) 014029 [[1911.00367](#)].
- [14] A. Kurz, T. Liu, P. Marquard and M. Steinhauser, *Hadronic contribution to the muon anomalous magnetic moment to next-to-next-to-leading order*, *Phys. Lett.* **B734** (2014) 144 [[1403.6400](#)].
- [15] K. Melnikov and A. Vainshtein, *Hadronic light-by-light scattering contribution to the muon anomalous magnetic moment revisited*, *Phys. Rev.* **D70** (2004) 113006 [[hep-ph/0312226](#)].
- [16] P. Masjuan and P. Sánchez-Puertas, *Pseudoscalar-pole contribution to the  $(g_\mu - 2)$ : a rational approach*, *Phys. Rev.* **D95** (2017) 054026 [[1701.05829](#)].

- [17] G. Colangelo, M. Hoferichter, M. Procura and P. Stoffer, *Dispersion relation for hadronic light-by-light scattering: two-pion contributions*, *JHEP* **04** (2017) 161 [[1702.07347](#)].
- [18] M. Hoferichter, B.-L. Hoid, B. Kubis, S. Leupold and S. P. Schneider, *Dispersion relation for hadronic light-by-light scattering: pion pole*, *JHEP* **10** (2018) 141 [[1808.04823](#)].
- [19] A. Gérardin, H. B. Meyer and A. Nyffeler, *Lattice calculation of the pion transition form factor with  $N_f = 2 + 1$  Wilson quarks*, *Phys. Rev.* **D100** (2019) 034520 [[1903.09471](#)].
- [20] J. Bijnens, N. Hermansson-Truedsson and A. Rodríguez-Sánchez, *Short-distance constraints for the HLbL contribution to the muon anomalous magnetic moment*, *Phys. Lett.* **B798** (2019) 134994 [[1908.03331](#)].
- [21] G. Colangelo, F. Hagelstein, M. Hoferichter, L. Laub and P. Stoffer, *Longitudinal short-distance constraints for the hadronic light-by-light contribution to  $(g - 2)_\mu$  with large- $N_c$  Regge models*, *JHEP* **03** (2020) 101 [[1910.13432](#)].
- [22] T. Blum, N. Christ, M. Hayakawa, T. Izubuchi, L. Jin, C. Jung et al., *The hadronic light-by-light scattering contribution to the muon anomalous magnetic moment from lattice QCD*, *Phys. Rev. Lett.* **124** (2020) 132002 [[1911.08123](#)].
- [23] G. Colangelo, M. Hoferichter, A. Nyffeler, M. Passera and P. Stoffer, *Remarks on higher-order hadronic corrections to the muon  $g - 2$* , *Phys. Lett.* **B735** (2014) 90 [[1403.7512](#)].
- [24] S. P. Martin and J. D. Wells, *Muon Anomalous Magnetic Dipole Moment in Supersymmetric Theories*, *Phys. Rev. D* **64** (2001) 035003 [[hep-ph/0103067](#)].
- [25] A. Czarnecki and W. J. Marciano, *The Muon anomalous magnetic moment: A Harbinger for 'new physics'*, *Phys. Rev. D* **64** (2001) 013014 [[hep-ph/0102122](#)].
- [26] D. Stockinger, *The Muon Magnetic Moment and Supersymmetry*, *J. Phys. G* **34** (2007) R45 [[hep-ph/0609168](#)].
- [27] J. Cao, Z. Heng, D. Li and J. M. Yang, *Current experimental constraints on the lightest Higgs boson mass in the constrained MSSM*, *Phys. Lett. B* **710** (2012) 665 [[1112.4391](#)].
- [28] Z. Kang,  *$H_{u,d}$ -messenger Couplings Address the  $\mu/B_\mu \setminus \mathcal{E} A_t/m_{H_u}^2$  Problem and  $(g - 2)_\mu$  Puzzle*, [1610.06024](#).
- [29] B. Zhu, R. Ding and T. Li, *Higgs mass and muon anomalous magnetic moment in the MSSM with gauge-gravity hybrid mediation*, *Phys. Rev. D* **96** (2017) 035029 [[1610.09840](#)].
- [30] T. T. Yanagida and N. Yokozaki, *Muon  $g - 2$  in MSSM gauge mediation revisited*, *Phys. Lett. B* **772** (2017) 409 [[1704.00711](#)].
- [31] K. Hagiwara, K. Ma and S. Mukhopadhyay, *Closing in on the chargino*

- contribution to the muon  $g-2$  in the MSSM: current LHC constraints, *Phys. Rev. D* **97** (2018) 055035 [[1706.09313](#)].
- [32] P. Cox, C. Han and T. T. Yanagida, *Muon  $g-2$  and dark matter in the minimal supersymmetric standard model*, *Phys. Rev. D* **98** (2018) 055015 [[1805.02802](#)].
  - [33] H. M. Tran and H. T. Nguyen, *GUT-inspired MSSM in light of muon  $g-2$  and LHC results at  $\sqrt{s} = 13$  TeV*, *Phys. Rev. D* **99** (2019) 035040 [[1812.11757](#)].
  - [34] B. P. Padley, K. Sinha and K. Wang, *Natural Supersymmetry, Muon  $g-2$ , and the Last Crevices for the Top Squark*, *Phys. Rev. D* **92** (2015) 055025 [[1505.05877](#)].
  - [35] A. Choudhury, L. Darmé, L. Roszkowski, E. M. Sessolo and S. Trojanowski, *Muon  $g-2$  and related phenomenology in constrained vector-like extensions of the MSSM*, *JHEP* **05** (2017) 072 [[1701.08778](#)].
  - [36] N. Okada and H. M. Tran, *125 GeV Higgs boson mass and muon  $g-2$  in 5D MSSM*, *Phys. Rev. D* **94** (2016) 075016 [[1606.05329](#)].
  - [37] X. Du and F. Wang, *NMSSM From Alternative Deflection in Generalized Deflected Anomaly Mediated SUSY Breaking*, *Eur. Phys. J. C* **78** (2018) 431 [[1710.06105](#)].
  - [38] X. Ning and F. Wang, *Solving the muon  $g-2$  anomaly within the NMSSM from generalized deflected AMSB*, *JHEP* **08** (2017) 089 [[1704.05079](#)].
  - [39] K. Wang, F. Wang, J. Zhu and Q. Jie, *The semi-constrained NMSSM in light of muon  $g-2$ , LHC, and dark matter constraints*, *Chin. Phys. C* **42** (2018) 103109 [[1811.04435](#)].
  - [40] J.-L. Yang, T.-F. Feng, Y.-L. Yan, W. Li, S.-M. Zhao and H.-B. Zhang, *Lepton-flavor violation and two loop electroweak corrections to  $(g-2)_\mu$  in the B-L symmetric SSM*, *Phys. Rev. D* **99** (2019) 015002 [[1812.03860](#)].
  - [41] C.-X. Liu, H.-B. Zhang, J.-L. Yang, S.-M. Zhao, Y.-B. Liu and T.-F. Feng, *Higgs boson decay  $h \rightarrow Z\gamma$  and muon magnetic dipole moment in the  $\mu\nu$ SSM*, *JHEP* **04** (2020) 002 [[2002.04370](#)].
  - [42] J. Cao, J. Lian, L. Meng, Y. Yue and P. Zhu, *Anomalous muon magnetic moment in the inverse seesaw extended next-to-minimal supersymmetric standard model*, *Phys. Rev. D* **101** (2020) 095009 [[1912.10225](#)].
  - [43] J. Cao, Y. He, J. Lian, D. Zhang and P. Zhu, *Electron and Muon Anomalous Magnetic Moments in the Inverse Seesaw Extended NMSSM*, [2102.11355](#).
  - [44] PLANCK collaboration, N. Aghanim et al., *Planck 2018 results. VI. Cosmological parameters*, *Astron. Astrophys.* **641** (2020) A6 [[1807.06209](#)].
  - [45] E. Bagnaschi et al., *Likelihood Analysis of the pMSSM11 in Light of LHC 13-TeV Data*, *Eur. Phys. J. C* **78** (2018) 256 [[1710.11091](#)].
  - [46] M. Chakraborti, S. Heinemeyer and I. Saha, *Improved  $(g-2)_\mu$  Measurements and Supersymmetry*, *Eur. Phys. J. C* **80** (2020) 984 [[2006.15157](#)].

- [47] M. Chakraborti, S. Heinemeyer and I. Saha, *The new "MUON G-2" Result and Supersymmetry*, [2104.03287](#).
- [48] M. Chakraborti, S. Heinemeyer and I. Saha, *Improved  $(g - 2)_\mu$  Measurements and Wino/Higgsino Dark Matter*, [2103.13403](#).
- [49] J. Cao, Y. He, L. Shang, W. Su and Y. Zhang, *Natural NMSSM after LHC Run I and the Higgsino dominated dark matter scenario*, *JHEP* **08** (2016) 037 [[1606.04416](#)].
- [50] U. Ellwanger, *Present Status and Future Tests of the Higgsino-Singlino Sector in the NMSSM*, *JHEP* **02** (2017) 051 [[1612.06574](#)].
- [51] Q.-F. Xiang, X.-J. Bi, P.-F. Yin and Z.-H. Yu, *Searching for Singlino-Higgsino Dark Matter in the NMSSM*, *Phys. Rev. D* **94** (2016) 055031 [[1606.02149](#)].
- [52] S. Baum, M. Carena, N. R. Shah and C. E. M. Wagner, *Higgs portals for thermal Dark Matter. EFT perspectives and the NMSSM*, *JHEP* **04** (2018) 069 [[1712.09873](#)].
- [53] U. Ellwanger and C. Hugonie, *The higgsino-singlino sector of the NMSSM: combined constraints from dark matter and the LHC*, *Eur. Phys. J. C* **78** (2018) 735 [[1806.09478](#)].
- [54] F. Domingo, J. S. Kim, V. M. Lozano, P. Martin-Ramiro and R. Ruiz de Austri, *Confronting the neutralino and chargino sector of the NMSSM with the multilepton searches at the LHC*, *Phys. Rev. D* **101** (2020) 075010 [[1812.05186](#)].
- [55] S. Baum, N. R. Shah and K. Freese, *The NMSSM is within Reach of the LHC: Mass Correlations & Decay Signatures*, *JHEP* **04** (2019) 011 [[1901.02332](#)].
- [56] M. van Beekveld, S. Caron and R. Ruiz de Austri, *The current status of fine-tuning in supersymmetry*, *JHEP* **01** (2020) 147 [[1906.10706](#)].
- [57] W. Abdallah, A. Chatterjee and A. Datta, *Revisiting singlino dark matter of the natural  $Z_3$ -symmetric NMSSM in the light of LHC*, *JHEP* **09** (2019) 095 [[1907.06270](#)].
- [58] J. Cao, L. Meng, Y. Yue, H. Zhou and P. Zhu, *Suppressing the scattering of WIMP dark matter and nucleons in supersymmetric theories*, *Phys. Rev. D* **101** (2020) 075003 [[1910.14317](#)].
- [59] M. Guchait and A. Roy, *Light Singlino Dark Matter at the LHC*, *Phys. Rev. D* **102** (2020) 075023 [[2005.05190](#)].
- [60] J. Cao, Y. He, L. Shang, W. Su, P. Wu and Y. Zhang, *Strong constraints of LUX-2016 results on the natural NMSSM*, *JHEP* **10** (2016) 136 [[1609.00204](#)].
- [61] J. Cao, Y. He, L. Shang, Y. Zhang and P. Zhu, *Current status of a natural NMSSM in light of LHC 13 TeV data and XENON-1T results*, *Phys. Rev. D* **99** (2019) 075020 [[1810.09143](#)].



- [62] H. Zhou, J. Cao, J. Lian and D. Zhang, *Singlino-dominated dark matter in  $Z_3$ -symmetric NMSSM*, *Phys. Rev. D* **104** (2021) 015017 [[2102.05309](#)].
- [63] M. Maniatis, *The Next-to-Minimal Supersymmetric extension of the Standard Model reviewed*, *Int. J. Mod. Phys. A* **25** (2010) 3505 [[0906.0777](#)].
- [64] U. Ellwanger, C. Hugonie and A. M. Teixeira, *The Next-to-Minimal Supersymmetric Standard Model*, *Phys. Rept.* **496** (2010) 1 [[0910.1785](#)].
- [65] U. Ellwanger, *Nonrenormalizable interactions from supergravity, quantum corrections and effective low-energy theories*, *Phys. Lett. B* **133** (1983) 187.
- [66] S. A. Abel, *Destabilizing divergences in the NMSSM*, *Nucl. Phys. B* **480** (1996) 55 [[hep-ph/9609323](#)].
- [67] C. F. Kolda, S. Pokorski and N. Polonsky, *Stabilized singlets in supergravity as a source of the  $\mu$  - parameter*, *Phys. Rev. Lett.* **80** (1998) 5263 [[hep-ph/9803310](#)].
- [68] C. Panagiotakopoulos and K. Tamvakis, *Stabilized NMSSM without domain walls*, *Phys. Lett. B* **446** (1999) 224 [[hep-ph/9809475](#)].
- [69] H. M. Lee, S. Raby, M. Ratz, G. G. Ross, R. Schieren, K. Schmidt-Hoberg et al., *A unique  $\mathbb{Z}_4^R$  symmetry for the MSSM*, *Phys. Lett. B* **694** (2011) 491 [[1009.0905](#)].
- [70] H. M. Lee, S. Raby, M. Ratz, G. G. Ross, R. Schieren, K. Schmidt-Hoberg et al., *Discrete  $R$  symmetries for the MSSM and its singlet extensions*, *Nucl. Phys. B* **850** (2011) 1 [[1102.3595](#)].
- [71] G. G. Ross and K. Schmidt-Hoberg, *The Fine-Tuning of the Generalised NMSSM*, *Nucl. Phys. B* **862** (2012) 710 [[1108.1284](#)].
- [72] G. G. Ross, K. Schmidt-Hoberg and F. Staub, *The Generalised NMSSM at One Loop: Fine Tuning and Phenomenology*, *JHEP* **08** (2012) 074 [[1205.1509](#)].
- [73] S. Ferrara, R. Kallosh, A. Linde, A. Marrani and A. Van Proeyen, *Superconformal Symmetry, NMSSM, and Inflation*, *Phys. Rev. D* **83** (2011) 025008 [[1008.2942](#)].
- [74] J. Cao, D. Li, J. Lian, Y. Yue and H. Zhou, *Singlino-dominated dark matter in general NMSSM*, *JHEP* **06** (2021) 176 [[2102.05317](#)].
- [75] W. G. Hollik, S. Liebler, G. Moortgat-Pick, S. Paßehr and G. Weiglein, *Phenomenology of the inflation-inspired NMSSM at the electroweak scale*, *Eur. Phys. J. C* **79** (2019) 75 [[1809.07371](#)].
- [76] W. G. Hollik, C. Li, G. Moortgat-Pick and S. Paasch, *Phenomenology of a Supersymmetric Model Inspired by Inflation*, *Eur. Phys. J. C* **81** (2021) 141 [[2004.14852](#)].
- [77] D. J. Miller, R. Nevzorov and P. M. Zerwas, *The Higgs sector of the next-to-minimal supersymmetric standard model*, *Nucl. Phys. B* **681** (2004) 3 [[hep-ph/0304049](#)].
- [78] J.-J. Cao, Z.-X. Heng, J. M. Yang, Y.-M. Zhang and J.-Y. Zhu, *A SM-like Higgs*

- near 125 GeV in low energy SUSY: a comparative study for MSSM and NMSSM, *JHEP* **03** (2012) 086 [[1202.5821](#)].
- [79] F. Domingo and U. Ellwanger, *Constraints from the Muon  $g-2$  on the Parameter Space of the NMSSM*, *JHEP* **07** (2008) 079 [[0806.0733](#)].
  - [80] S. Heinemeyer, D. Stockinger and G. Weiglein, *Two loop SUSY corrections to the anomalous magnetic moment of the muon*, *Nucl. Phys. B* **690** (2004) 62 [[hep-ph/0312264](#)].
  - [81] S. Heinemeyer, D. Stockinger and G. Weiglein, *Electroweak and supersymmetric two-loop corrections to  $(g-2)(\mu)$* , *Nucl. Phys. B* **699** (2004) 103 [[hep-ph/0405255](#)].
  - [82] H. Fargnoli, C. Gnendiger, S. Paßehr, D. Stöckinger and H. Stöckinger-Kim, *Two-loop corrections to the muon magnetic moment from fermion/sfermion loops in the MSSM: detailed results*, *JHEP* **02** (2014) 070 [[1311.1775](#)].
  - [83] H. G. Fargnoli, C. Gnendiger, S. Paßehr, D. Stöckinger and H. Stöckinger-Kim, *Non-decoupling two-loop corrections to  $(g-2)_\mu$  from fermion/sfermion loops in the MSSM*, *Phys. Lett. B* **726** (2013) 717 [[1309.0980](#)].
  - [84] P. von Weitershausen, M. Schafer, H. Stockinger-Kim and D. Stockinger, *Photonic SUSY Two-Loop Corrections to the Muon Magnetic Moment*, *Phys. Rev. D* **81** (2010) 093004 [[1003.5820](#)].
  - [85] A. Arhrib and S. Baek, *Two loop Barr-Zee type contributions to  $(g-2)(\mu)$  in the MSSM*, *Phys. Rev. D* **65** (2002) 075002 [[hep-ph/0104225](#)].
  - [86] S.-M. Zhao, F. Wang, B. Chen, T.-F. Feng, H.-B. Zhang, X.-D. Guo et al., *Some two-loop contributions to muon magnetic dipole moment in the CP-violating MSSM*, *Mod. Phys. Lett. A* **28** (2013) 1350173.
  - [87] S.-M. Zhao, T.-F. Feng, T. Li, X.-Q. Li and K.-S. Sun, *The supersymmetric two-loop corrections to muon magnetic dipole moments in the CP-violating MSSM*, *Mod. Phys. Lett. A* **27** (2012) 1250045.
  - [88] D. Chang, W.-F. Chang, C.-H. Chou and W.-Y. Keung, *Large two loop contributions to  $g-2$  from a generic pseudoscalar boson*, *Phys. Rev. D* **63** (2001) 091301 [[hep-ph/0009292](#)].
  - [89] H. G. Fargnoli, C. Gnendiger, S. Paßehr, D. Stöckinger and H. Stöckinger-Kim, *Two-loop corrections to  $(g-2)_\mu$  in the SM and MSSM*, *PoS* **LL2014** (2014) 067.
  - [90] D. Stockinger, *Supersymmetric two-loop contributions to the anomalous magnetic moment of the muon*, *Nucl. Phys. B Proc. Suppl.* **135** (2004) 311 [[hep-ph/0406306](#)].
  - [91] T.-F. Feng, L. Sun and X.-Y. Yang, *Electroweak and supersymmetric two-loop corrections to lepton anomalous magnetic and electric dipole moments*, *Nucl. Phys. B* **800** (2008) 221 [[0805.1122](#)].
  - [92] S.-M. Zhao, L.-H. Su, X.-X. Dong, T.-T. Wang and T.-F. Feng, *Study muon  $g-2$  at two loop level in the  $U(1)_X$  SSM*, [2107.03571](#).



- [93] T. Moroi, *The Muon anomalous magnetic dipole moment in the minimal supersymmetric standard model*, *Phys. Rev. D* **53** (1996) 6565 [[hep-ph/9512396](#)].
- [94] W. Hollik, J. I. Illana, S. Rigolin and D. Stockinger, *One loop MSSM contribution to the weak magnetic dipole moments of heavy fermions*, *Phys. Lett. B* **416** (1998) 345 [[hep-ph/9707437](#)].
- [95] P. Athron, M. Bach, H. G. Fargnoli, C. Gnendiger, R. Greifenhagen, J.-h. Park et al., *GM2Calc: Precise MSSM prediction for  $(g - 2)$  of the muon*, *Eur. Phys. J. C* **76** (2016) 62 [[1510.08071](#)].
- [96] M. Endo, K. Hamaguchi, S. Iwamoto and T. Kitahara, *Supersymmetric interpretation of the muon  $g - 2$  anomaly*, *JHEP* **07** (2021) 075 [[2104.03217](#)].
- [97] K. Griest and D. Seckel, *Three exceptions in the calculation of relic abundances*, *Phys. Rev. D* **43** (1991) 3191.
- [98] XENON collaboration, E. Aprile et al., *Dark Matter Search Results from a One Ton-Year Exposure of XENON1T*, *Phys. Rev. Lett.* **121** (2018) 111302 [[1805.12562](#)].
- [99] PANDAX-II collaboration, Q. Wang et al., *Results of dark matter search using the full PandaX-II exposure*, *Chin. Phys. C* **44** (2020) 125001 [[2007.15469](#)].
- [100] PARTICLE DATA GROUP collaboration, M. Tanabashi et al., *Review of Particle Physics*, *Phys. Rev. D* **98** (2018) 030001.
- [101] R. E. Kass and A. E. Raftery, *Bayes Factors*, *J. Am. Statist. Assoc.* **90** (1995) 773.
- [102] M. Badziak, M. Olechowski and P. Szczerbiak, *Blind spots for neutralinos in NMSSM with light singlet scalar*, *PoS PLANCK2015* (2015) 130 [[1601.00768](#)].
- [103] A. Pierce, N. R. Shah and K. Freese, *Neutralino Dark Matter with Light Staus*, [1309.7351](#).
- [104] M. Badziak, M. Olechowski and P. Szczerbiak, *Blind spots for neutralino dark matter in the NMSSM*, *JHEP* **03** (2016) 179 [[1512.02472](#)].
- [105] M. Badziak, M. Olechowski and P. Szczerbiak, *Spin-dependent constraints on blind spots for thermal singlino-higgsino dark matter with(out) light singlets*, *JHEP* **07** (2017) 050 [[1705.00227](#)].
- [106] F. Feroz, M. P. Hobson and M. Bridges, *MultiNest: an efficient and robust Bayesian inference tool for cosmology and particle physics*, *Mon. Not. Roy. Astron. Soc.* **398** (2009) 1601 [[0809.3437](#)].
- [107] F. Feroz, M. P. Hobson, E. Cameron and A. N. Pettitt, *Importance Nested Sampling and the MultiNest Algorithm*, *Open J. Astrophys.* **2** (2019) 10 [[1306.2144](#)].
- [108] F. Staub, *SARAH*, [0806.0538](#).
- [109] F. Staub, *SARAH 3.2: Dirac Gauginos, UFO output, and more*, *Comput. Phys. Commun.* **184** (2013) 1792 [[1207.0906](#)].

- [110] F. Staub, *SARAH 4 : A tool for (not only SUSY) model builders*, *Comput. Phys. Commun.* **185** (2014) 1773 [[1309.7223](#)].
- [111] F. Staub, *Exploring new models in all detail with SARAH*, *Adv. High Energy Phys.* **2015** (2015) 840780 [[1503.04200](#)].
- [112] W. Porod, *SPheno, a program for calculating supersymmetric spectra, SUSY particle decays and SUSY particle production at  $e^+ e^-$  colliders*, *Comput. Phys. Commun.* **153** (2003) 275 [[hep-ph/0301101](#)].
- [113] W. Porod and F. Staub, *SPheno 3.1: Extensions including flavour, CP-phases and models beyond the MSSM*, *Comput. Phys. Commun.* **183** (2012) 2458 [[1104.1573](#)].
- [114] W. Porod, F. Staub and A. Vicente, *A Flavor Kit for BSM models*, *Eur. Phys. J. C* **74** (2014) 2992 [[1405.1434](#)].
- [115] G. Belanger, F. Boudjema, A. Pukhov and A. Semenov, *MicrOMEGAs: A Program for calculating the relic density in the MSSM*, *Comput. Phys. Commun.* **149** (2002) 103 [[hep-ph/0112278](#)].
- [116] G. Belanger, F. Boudjema, C. Hugonie, A. Pukhov and A. Semenov, *Relic density of dark matter in the NMSSM*, *JCAP* **09** (2005) 001 [[hep-ph/0505142](#)].
- [117] G. Belanger, F. Boudjema, A. Pukhov and A. Semenov, *MicrOMEGAs 2.0: A Program to calculate the relic density of dark matter in a generic model*, *Comput. Phys. Commun.* **176** (2007) 367 [[hep-ph/0607059](#)].
- [118] G. Belanger, F. Boudjema, A. Pukhov and A. Semenov, *micrOMEGAs: A Tool for dark matter studies*, *Nuovo Cim. C* **033N2** (2010) 111 [[1005.4133](#)].
- [119] G. Belanger, F. Boudjema, A. Pukhov and A. Semenov, *micrOMEGAs\_3: A program for calculating dark matter observables*, *Comput. Phys. Commun.* **185** (2014) 960 [[1305.0237](#)].
- [120] D. Barducci, G. Belanger, J. Bernon, F. Boudjema, J. Da Silva, S. Kraml et al., *Collider limits on new physics within micrOMEGAs\_4.3*, *Comput. Phys. Commun.* **222** (2018) 327 [[1606.03834](#)].
- [121] P. Bechtle, S. Heinemeyer, O. Stål, T. Stefaniak and G. Weiglein, *Probing the Standard Model with Higgs signal rates from the Tevatron, the LHC and a future ILC*, *JHEP* **11** (2014) 039 [[1403.1582](#)].
- [122] P. Bechtle, S. Heinemeyer, O. Stal, T. Stefaniak and G. Weiglein, *Applying Exclusion Likelihoods from LHC Searches to Extended Higgs Sectors*, *Eur. Phys. J. C* **75** (2015) 421 [[1507.06706](#)].
- [123] XENON collaboration, E. Aprile et al., *Constraining the spin-dependent WIMP-nucleon cross sections with XENON1T*, *Phys. Rev. Lett.* **122** (2019) 141301 [[1902.03234](#)].
- [124] C. K. Khosa, S. Kraml, A. Lessa, P. Neuhuber and W. Waltenberger, *SModelS database update v1.2.3*, [2005.00555](#).

- [125] J. E. Camargo-Molina, B. O’Leary, W. Porod and F. Staub, **Vevacious: A Tool For Finding The Global Minima Of One-Loop Effective Potentials With Many Scalars**, *Eur. Phys. J. C* **73** (2013) 2588 [[1307.1477](#)].
- [126] J. E. Camargo-Molina, B. Garbrecht, B. O’Leary, W. Porod and F. Staub, *Constraining the Natural MSSM through tunneling to color-breaking vacua at zero and non-zero temperature*, *Phys. Lett. B* **737** (2014) 156 [[1405.7376](#)].
- [127] J. Beuria, U. Chattopadhyay, A. Datta and A. Dey, *Exploring viable vacua of the  $Z_3$ -symmetric NMSSM*, *JHEP* **04** (2017) 024 [[1612.06803](#)].
- [128] T. Kitahara and T. Yoshinaga, *Stau with Large Mass Difference and Enhancement of the Higgs to Diphoton Decay Rate in the MSSM*, *JHEP* **05** (2013) 035 [[1303.0461](#)].
- [129] M. Endo, K. Hamaguchi, T. Kitahara and T. Yoshinaga, *Probing Bino contribution to muon  $g - 2$* , *JHEP* **11** (2013) 013 [[1309.3065](#)].
- [130] M. Carena, D. Garcia, U. Nierste and C. E. M. Wagner, *Effective Lagrangian for the  $\bar{t}bH^+$  interaction in the MSSM and charged Higgs phenomenology*, *Nucl. Phys. B* **577** (2000) 88 [[hep-ph/9912516](#)].
- [131] ATLAS collaboration, G. Aad et al., *Combined measurements of Higgs boson production and decay using up to 80  $\text{fb}^{-1}$  of proton-proton collision data at  $\sqrt{s} = 13$  TeV collected with the ATLAS experiment*, *Phys. Rev. D* **101** (2020) 012002 [[1909.02845](#)].
- [132] ATLAS collaboration, G. Aad et al., *A search for the dimuon decay of the Standard Model Higgs boson with the ATLAS detector*, *Phys. Lett. B* **812** (2021) 135980 [[2007.07830](#)].
- [133] M. Pospelov, A. Ritz and M. B. Voloshin, *Secluded WIMP Dark Matter*, *Phys. Lett. B* **662** (2008) 53 [[0711.4866](#)].
- [134] J. L. Hintze and R. D. Nelson, *Violin plots: a box plot-density trace synergism*, *The American Statistician* **52** (1998) 181.
- [135] W. Beenakker, R. Hopker and M. Spira, *PROSPINO: A Program for the production of supersymmetric particles in next-to-leading order QCD*, [hep-ph/9611232](#).
- [136] J. Alwall, M. Herquet, F. Maltoni, O. Mattelaer and T. Stelzer, *MadGraph 5 : Going Beyond*, *JHEP* **06** (2011) 128 [[1106.0522](#)].
- [137] E. Conte, B. Fuks and G. Serret, *MadAnalysis 5, A User-Friendly Framework for Collider Phenomenology*, *Comput. Phys. Commun.* **184** (2013) 222 [[1206.1599](#)].
- [138] T. Sjöstrand, S. Ask, J. R. Christiansen, R. Corke, N. Desai, P. Ilten et al., *An introduction to PYTHIA 8.2*, *Comput. Phys. Commun.* **191** (2015) 159 [[1410.3012](#)].
- [139] M. Drees, H. Dreiner, D. Schmeier, J. Tattersall and J. S. Kim, *CheckMATE: Confronting your Favourite New Physics Model with LHC Data*, *Comput. Phys. Commun.* **187** (2015) 227 [[1312.2591](#)].

- [140] D. Dercks, N. Desai, J. S. Kim, K. Rolbiecki, J. Tattersall and T. Weber, *CheckMATE 2: From the model to the limit*, *Comput. Phys. Commun.* **221** (2017) 383 [[1611.09856](#)].
- [141] J. S. Kim, D. Schmeier, J. Tattersall and K. Rolbiecki, *A framework to create customised LHC analyses within CheckMATE*, *Comput. Phys. Commun.* **196** (2015) 535 [[1503.01123](#)].
- [142] DELPHES 3 collaboration, J. de Favereau, C. Delaere, P. Demin, A. Giammanco, V. Lemaître, A. Mertens et al., *DELPHES 3, A modular framework for fast simulation of a generic collider experiment*, *JHEP* **02** (2014) 057 [[1307.6346](#)].
- [143] ATLAS collaboration, G. Aad et al., *Search for electroweak production of charginos and sleptons decaying into final states with two leptons and missing transverse momentum in  $\sqrt{s} = 13$  TeV pp collisions using the ATLAS detector*, *Eur. Phys. J. C* **80** (2020) 123 [[1908.08215](#)].
- [144] ATLAS collaboration, G. Aad et al., *Search for chargino-neutralino production with mass splittings near the electroweak scale in three-lepton final states in  $\sqrt{s}=13$  TeV pp collisions with the ATLAS detector*, *Phys. Rev. D* **101** (2020) 072001 [[1912.08479](#)].
- [145] ATLAS collaboration, G. Aad et al., *Search for direct production of electroweakinos in final states with one lepton, missing transverse momentum and a Higgs boson decaying into two b-jets in pp collisions at  $\sqrt{s} = 13$  TeV with the ATLAS detector*, *Eur. Phys. J. C* **80** (2020) 691 [[1909.09226](#)].
- [146] CMS collaboration, A. M. Sirunyan et al., *Combined search for electroweak production of charginos and neutralinos in proton-proton collisions at  $\sqrt{s} = 13$  TeV*, *JHEP* **03** (2018) 160 [[1801.03957](#)].
- [147] CMS collaboration, A. M. Sirunyan et al., *Search for supersymmetry in final states with two oppositely charged same-flavor leptons and missing transverse momentum in proton-proton collisions at  $\sqrt{s} = 13$  TeV*, *JHEP* **04** (2021) 123 [[2012.08600](#)].
- [148] ATLAS collaboration, G. Aad et al., *Search for chargino–neutralino pair production in final states with three leptons and missing transverse momentum in  $\sqrt{s} = 13$  TeV pp collisions with the ATLAS detector*, [2106.01676](#).
- [149] S. Heinemeyer and C. Schappacher, *Chargino and neutralino production at  $e^+e^-$  colliders in the complex MSSM: a full one-loop analysis*, *Eur. Phys. J. C* **77** (2017) 649 [[1704.07627](#)].
- [150] L. Linssen, A. Miyamoto, M. Stanitzki and H. Weerts, *Physics and detectors at clic: Clic conceptual design report*, 2012.
- [151] CLIC DETECTOR, PHYSICS STUDY collaboration, H. Abramowicz et al., *Physics at the CLIC  $e+e^-$  Linear Collider – Input to the Snowmass process 2013*, in *Community Summer Study 2013: Snowmass on the Mississippi*, 7, 2013, [1307.5288](#).

- [152] A. Arbey et al., *Physics at the  $e^+e^-$  Linear Collider*, *Eur. Phys. J. C* **75** (2015) 371 [[1504.01726](#)].
- [153] CLICDP, CLIC collaboration, T. K. Charles et al., *The Compact Linear Collider (CLIC) - 2018 Summary Report*, [1812.06018](#).
- [154] M. Endo, K. Hamaguchi, S. Iwamoto and T. Kitahara, *Muon  $g-2$  vs LHC Run 2 in supersymmetric models*, *JHEP* **04** (2020) 165 [[2001.11025](#)].
- [155] ATLAS COLLABORATION collaboration, *Prospects for searches for staus, charginos and neutralinos at the high luminosity LHC with the ATLAS Detector*, tech. rep., CERN, Geneva, Dec, 2018.
- [156] X. Cid Vidal et al., *Report from Working Group 3: Beyond the Standard Model physics at the HL-LHC and HE-LHC*, *CERN Yellow Rep. Monogr.* **7** (2019) 585 [[1812.07831](#)].
- [157] L. Beresford and J. Liu, *Search Strategy for Sleptons and Dark Matter Using the LHC as a Photon Collider*, *Phys. Rev. Lett.* **123** (2019) 141801 [[1811.06465](#)].
- [158] CMS collaboration, A. M. Sirunyan et al., *Searches for pair production of charginos and top squarks in final states with two oppositely charged leptons in proton-proton collisions at  $\sqrt{s} = 13$  TeV*, *JHEP* **11** (2018) 079 [[1807.07799](#)].
- [159] CMS collaboration, A. M. Sirunyan et al., *Search for supersymmetric partners of electrons and muons in proton-proton collisions at  $\sqrt{s} = 13$  TeV*, *Phys. Lett. B* **790** (2019) 140 [[1806.05264](#)].
- [160] CMS collaboration, A. M. Sirunyan et al., *Search for supersymmetry with Higgs boson to diphoton decays using the razor variables at  $\sqrt{s} = 13$  TeV*, *Phys. Lett. B* **779** (2018) 166 [[1709.00384](#)].
- [161] CMS collaboration, A. M. Sirunyan et al., *Search for electroweak production of charginos and neutralinos in multilepton final states in proton-proton collisions at  $\sqrt{s} = 13$  TeV*, *JHEP* **03** (2018) 166 [[1709.05406](#)].
- [162] CMS collaboration, A. M. Sirunyan et al., *Search for new phenomena in final states with two opposite-charge, same-flavor leptons, jets, and missing transverse momentum in  $pp$  collisions at  $\sqrt{s} = 13$  TeV*, *JHEP* **03** (2018) 076 [[1709.08908](#)].
- [163] ATLAS collaboration, M. Aaboud et al., *Search for electroweak production of supersymmetric particles in final states with two or three leptons at  $\sqrt{s} = 13$  TeV with the ATLAS detector*, *Eur. Phys. J. C* **78** (2018) 995 [[1803.02762](#)].
- [164] ATLAS collaboration, M. Aaboud et al., *Search for chargino and neutralino production in final states with a Higgs boson and missing transverse momentum at  $\sqrt{s} = 13$  TeV with the ATLAS detector*, *Phys. Rev. D* **100** (2019) 012006 [[1812.09432](#)].
- [165] ATLAS collaboration, M. Aaboud et al., *Search for chargino-neutralino production using recursive jigsaw reconstruction in final states with two or three charged*

- leptons in proton-proton collisions at  $\sqrt{s} = 13$  TeV with the ATLAS detector*, *Phys. Rev. D* **98** (2018) 092012 [[1806.02293](#)].
- [166] S. Kraml, S. Kulkarni, U. Laa, A. Lessa, W. Magerl, D. Proschofsky-Spindler et al., *SModelS: a tool for interpreting simplified-model results from the LHC and its application to supersymmetry*, *Eur. Phys. J. C* **74** (2014) 2868 [[1312.4175](#)].
  - [167] F. Ambrogio, S. Kraml, S. Kulkarni, U. Laa, A. Lessa, V. Magerl et al., *SModelS v1.1 user manual: Improving simplified model constraints with efficiency maps*, *Comput. Phys. Commun.* **227** (2018) 72 [[1701.06586](#)].
  - [168] J. Dutta, S. Kraml, A. Lessa and W. Waltenberger, *SModelS extension with the CMS supersymmetry search results from Run 2*, *LHEP* **1** (2018) 5 [[1803.02204](#)].
  - [169] J. Heisig, S. Kraml and A. Lessa, *Constraining new physics with searches for long-lived particles: Implementation into SModelS*, *Phys. Lett. B* **788** (2019) 87 [[1808.05229](#)].
  - [170] G. Alguero, S. Kraml and W. Waltenberger, *A SModelS interface for pyhf likelihoods*, *Comput. Phys. Commun.* **264** (2021) 107909 [[2009.01809](#)].